direction of the main symmetry axis of the crystal is not changed in the phase transition, remaining parallel in the domains below and above the phase transition. The main difference between the twin components relates to in which layer the triangle formed by the O(2) atoms is rotated.

Analysis of the thermal vibration parameters of the atoms provided the obvious correlations between vibrational amplitudes and the strength and direction of the chemical bonds in the structure. Thus the semi-minor axes u_1 of the ellipsoids for the O(1) and O(2) atoms are aligned along the strongest Cr—O bonds. Both O atoms show strong anisotropy of thermal vibrations and the u_2 and u_3 parameters describing their thermal motion in the planes of the perpendicular Cr—O bonds have much larger values than u_1. Increasing temperature and the phase transition are accompanied by reduction of the anisotropy of thermal vibration for the Cr atom and simultaneous levelling of the thermal parameters of the O(1) and O(2) atoms along the Cr—O bonds.

Fig. 8 depicts the temperature dependence of the thermal parameters for $RbLiCrO_4$ (the equivalent isotropic thermal parameters B_{eq} for the Rb and Cr atoms with a small anisotropy of thermal vibration and parameters u_i^2 for the O atoms). Parameters of the Li atom are not shown because of their low accuracy. In comparison with the values at 293 K, the thermal parameters of all the atoms at 428 K increase almost proportionally to the changes in absolute temperature. As the phase transition is approached (T_{pt} = 550 K) the thermal parameters of $RbLiCrO_4$ increase drastically. This seems to be associated with the temperature dependence of the force constants in the vicinity of the phase-transition temperature. But the increase in the u_2^2 and u_3^2 parameters of the O(2) atom which rotates during the process of phase transition is clearly seen even against a background of such a drastic increase in thermal parameters. The anharmonic parameters of the O(2) atom obtained for the G_2 phase also indicate some 'softening' of the effective potential for this atom. Finer details in the behaviour of the thermal parameters of atoms in the structures of the type considered above can be established in separate neutron diffraction experiments.

The authors are grateful to Professor V. I. Simonov for many helpful discussions.

References

BECKER, P. J. & COPPENS, P. (1974). *Acta Cryst.* A**30**, 129–147.

BHAKAY-TAMHANE, S., SEQUEIRA, A. & CHIDAMBARAM, R. (1984). *Acta Cryst.* C**40**, 1648–1651.

CATTI, M. & FERRARIS, G. (1976). *Acta Cryst.* A**32**, 163–165.

DONNAY, G. & DONNAY, J. D. (1974). *Can. Mineral.* **12**, 422–425.

HAMILTON, W. C. (1965). *Acta Cryst.* **18**, 502–510.

KARPPINEN, M., LUNDGREN, J. O. & LIMINGA, R. (1983). *Acta Cryst.* C**39**, 34–38.

KLAPPER, H., HAHN, TH. & CHUNG, S. J. (1987). *Acta Cryst.* B**43**, 147–159.

KRUGLIK, A. I., MEL'NIKOVA, S. V., ALEKSANDROV, K. S. & GRANKINA, V. A. (1990). *Fiz. Tverd. Tela*, **32**, 3029.

KRUGLIK, A. I., MEL'NIKOVA, S. V., TOLOCHKO, B. P., MAKAROVA, I. P. & ALEKSANDROV, K. S. (1991). Preprint No. 680F of the L. V. Kirenskii Institute of Physics of the Siberian Division of the USSR Academy of Sciences, Krasnoyarsk, Russia.

MURADYAN, L. A., SIROTA, M. I., MAKAROVA, I. P. & SIMONOV, V. I. (1985). *Kristallografiya*, **30**, 258–266.

SCHULZ, H., ZUCKER, U. & FRECH, R. (1985). *Acta Cryst.* B**41**, 21–26.

SIROTA, M. I. & MAKSIMOV, B. A. (1984). *Kristallografiya*, **29**, 34–38.

ZHANG, P. L., YAN, Q. W. & BOUCHERLE, J. X. (1988). *Acta Cryst.* C**44**, 592–595.

ZUCKER, U. H., PERENTHALER, E., KUHS, W. F., BACHMANN, R. & SCHULZ, H. (1983). *J. Appl. Cryst.* **16**, 358.

Acta Cryst. (1993). B**49**, 28–56

Structural Relations in Copper Oxysalt Minerals. I. Structural Hierarchy

BY RAY K. EBY* AND FRANK C. HAWTHORNE

Department of Geological Sciences, University of Manitoba, Winnipeg, Manitoba, Canada R3T 2N2

(*Received* 11 *September* 1990; *accepted* 2 *July* 1992)

Abstract

A hierarchical structural classification is developed for the copper oxysalt minerals, based on the polymerization of coordination polyhedra of higher bond valences, and focusing specifically on [3]-, [4]-, [5]- and [6]-coordinate polyhedra. The nature of copper oxysalt structures is complicated by the extremely distorted coordinations often occurring around the Cu^{2+} cation, a result of the well-known Jahn–Teller

* Present address: Department of Geology, University of Toronto, Toronto, Ontario, Canada M55 1A7.

0108-7681/93/010028-29$06.00

effect. Although this is widely recognized at the qualitative level, it has led to a very inconsistent assignment of coordination numbers to Cu^{2+} in minerals. While this seems like a minor point, it has made intercomparison of copper oxysalt structures generally difficult to impossible. Here we re-examine these structures, assigning octahedral coordination to Cu^{2+} wherever possible; in the majority of structures this can be done. This allows a consistent hierarchical organization scheme to be developed for these structures, and also allows structural comparison with other triangular/tetrahedral/octahedral structures. Cu^{2+} shows octahedral, square-pyramidal, triangular-bipyramidal, square-planar, trigonal-prismatic and augmented-octahedral ([7]-fold) coordinations in oxysalt minerals. Octahedral coordination is by far the most common. The distribution of octahedral bond lengths is distinctly bimodal, with maxima at 1.97 and 2.44 Å and a frequency of 2:1; this is compatible with the usual Jahn–Teller argument concerning bond-length distributions in Cu^{2+} compounds, the [4 + 2]-coordination. There are a few instances of regular octahedral coordination, sometimes (but not always) forced by symmetry. Such examples are either at a position of very low multiplicity, or are associated with partially occupied sites. Only one example of [2 + 4]-coordination occurs, again at a site of low multiplicity. These unusual coordinations are generally associated with some type of disorder. Square-pyramidal and triangular-bipyramidal coordinations are also common, but do not show the distortions from regularity (with regard to bond length) that characterize octahedral coordination. The overall distribution of compositions is centered on an *o:t* (octahedra:tetrahedra or triangles) ratio of 1:1. For chain and sheet structures, $o:t < 1:1$; the framework structures show a wider distribution, but $o:t > 1:1$ predominates.

Introduction

Divalent copper oxysalt minerals have long been considered an enigma among minerals. They are rarely isostructural with non-Cu^{2+} oxysalts, and are difficult to rationalize within such traditional structural themes as anion close packing. As described in most structural papers, Cu^{2+} shows a bewildering variety of coordinations: square planar, square pyramidal, triangular bipyramidal and octahedral. Even within a specific coordination type, deviations from the ideal holosymmetric arrangement vary from negligible to extreme. In addition, these minerals are often hydrated and our understanding of hydrated structures in general has not progressed at the same rate as for anhydrous compounds.

Electronic degeneracy in $^{[6]}Cu^{2+}$ structures

The reason for the problem with Cu^{2+} minerals is well known. When octahedrally coordinated, Cu^{2+} spontaneously induces a local geometrical distortion due to an electronic orbital degeneracy in the holosymmetric state. The Jahn–Teller theorem (Jahn & Teller, 1937) shows that any non-linear polyatomic *molecule* with an electronic orbital degeneracy is unstable relative to any local distortion that splits the degenerate state. The molecule thus spontaneously distorts to relieve this instability; such an effect is known as a Jahn–Teller distortion. The strongly distorted Cu^{2+} coordination polyhedra in minerals (and other synthetic solids) have been widely rationalized as being due to this Jahn–Teller effect. In fact, the Jahn–Teller effect refers to this distortion in *molecules*; in solids, the effect has been discussed (but not in Cu^{2+} compounds) as the *Peierls distortion*. The similarities between these two effects are examined by Burdett (1982) and Albright, Burdett & Whangbo (1985). Although this distinction may seem at first to be rather nitpicking, in this distinction lies the key to understanding the Cu^{2+} oxysalts. The Jahn–Teller effect refers to a molecular or *local* effect, whereas the Cu^{2+} oxysalt minerals are extended structures with translational symmetry, and solely local arguments are not sufficient to explain their complexity. We need to consider the following points:

(i) the electronic requirement for a distorted (octahedral) coordination;

(ii) the satisfaction of local bond-valence requirements (Brown, 1981);

(iii) the requirement that the crystal (by definition) be periodic.

These three factors must interact to produce the observed arrangement, and omission of any of these factors in the consideration of Cu^{2+} oxysalts must lead to an inadequate rationalization of their structures. Here we attempt to produce a coherent structural hierarchy for the copper oxysalt minerals; with this in place, the interaction of the three factors noted above can be examined. Future work includes a quantitative examination of the Jahn–Teller effect in $(Cu^{2+}\varphi_n)$ (φ = unspecified ligand) clusters *via ab initio* UHF MO cluster calculations, the development of anisotropic Cu—φ potentials for use in molecular mechanics calculations, and an examination of Jahn–Teller-driven phase transitions.

Structural hierarchies

Hawthorne (1983) has proposed that mineral structures can be ordered (or classified) according to the polymerization of those coordination polyhedra with higher bond valences, and has applied this idea to the structural hierarchy of minerals with

$^{[6]}M^{[4]}T_2\varphi_n$ and $^{[6]}M_x{}^{[3]}T_y\varphi_z$ stoichiometries (Hawthorne, 1985*a*, 1986*a*). Here we use these ideas to set up a structure hierarchy for the Cu^{2+} oxysalt minerals. An important part of this process is to present consistent graphical representations of these structures in terms of ($Cu\varphi_6$) polyhedra, as without this graphical information, the way in which the structure accommodates the local relaxation of the ($Cu\varphi_6$) group cannot be examined.

Structural mechanisms of electronic relaxation

The ideas outlined above provide a conceptual framework within which such structures may be represented and interpreted. However, in the case of the Cu^{2+} oxysalts, this is not quite sufficient, as it does not deal with the aspects that relate to the very distorted local environment of Cu^{2+}. From an *a priori* viewpoint, we may identify three principal ways in which the electronic degeneracy of Cu^{2+} may be lifted in a periodic structure:

(i) The coordination of the Cu^{2+} is *intrinsically* [4] or [5]; that is, there are no other anions that could possibly be considered as producing [6]-coordination around the Cu^{2+} under a small displacement.

(ii) The connectivity of the structure *forces* the $^{[6]}Cu^{2+}—\varphi$ bonds to be extremely distorted; thus the structure is incompatible with holosymmetric octahedra.

(iii) The structural connectivity is compatible with holosymmetrical octahedra, but the very distorted octahedral coordination results from a strong electron–phonon interaction. The resulting Cu^{2+} coordination may or may not be octahedral, but the *ideal* prototype structure (*i.e.* without the electron–phonon interaction) has regular octahedral coordination around the Cu^{2+} position.

In order to understand the energetics of Cu^{2+} oxysalts, it is important to be able to distinguish between these three different situations. This provides the principal reason for this graphical reconsideration of the Cu^{2+} oxysalt minerals given here.

As outlined above, there are four basic coordinations for Cu^{2+}: square planar, triangular bipyramidal, square pyramidal and octahedral. All of these can be considered as being derived from a holosymmetric octahedral arrangement by displacement of the ligands (coordination number is changed by extension of a $Cu—\varphi$ distance until the bonding interaction becomes negligible). Thus we can conceive of producing these coordination geometries from an ideal octahedral arrangement *via* an electron–phonon interaction.

For any structure with [4]- or [5]-coordinate Cu^{2+} [as described by the original author(s)], there are several questions of interest:

(i) Is the Cu^{2+} actually [6]-coordinate (*i.e.* underestimated by the original author)?

(ii) Is the structure compatible with [6]-coordinate Cu^{2+}? That is, can a distortion of the observed arrangement bring a fifth and/or sixth anion into the coordination sphere of Cu^{2+} such that its coordination becomes octahedral without altering any other aspect of the bond connectivity of the structure?

If (i) or (ii) is the case, then we can fit the structure into our normal hierarchy of tetrahedral/octahedral structures, and examine the way in which the local distortion around the Cu^{2+} has affected the polyhedral connectivity. Moreover, we can also identify those structures in which the Cu^{2+} coordination is *intrinsically* [4]- or [5]-coordinate.

Notation

For the purpose of discussion, we need a simple shorthand that can easily represent the different types of polyhedral connectivities; this will avoid some of the rather cumbersome expressions that would otherwise occur. The following notation is adopted: M = an octahedrally coordinated cation; T = a triangularly or tetrahedrally coordinated cation; φ = an unspecified ligand.

Linkage between polyhedra will be indicated by hyphens between the symbols, the number of hyphens corresponding to the number of common ligands. Thus $M—M$ represents corner sharing between octahedra, and $M{=}M$ represents edge sharing between octahedra. An $M—T$ chain is a chain in which the only linkage is corner sharing between octahedra and tetrahedra; an $M{=}T$ chain is a chain in which the only linkage is edge sharing between octahedra and tetrahedra. Polyhedra are denoted by round brackets: octahedron = ($M\varphi_6$), tetrahedron = ($T\varphi_4$). Connected arrays of polyhedra are denoted by square brackets: a corner-sharing octahedral chain of the form $\cdots M—M—M\cdots$ is [$M\varphi_5$], an edge-sharing octahedral chain of the form $\cdots M{=}M{=}M\cdots$ is [$M\varphi_4$], a corner-sharing octahedral–tetrahedral chain of the form $\cdots M—T—M—T\cdots$ is [$M(T\varphi_4)\varphi_4$]. Crystallographic data, chemical data and references to the original structural descriptions are given in Tables 1–5.

Isolated polyhedral structures

Copper oxysalt structures that are based on isolated polyhedra are listed in Table 1; it is notable that they are all sulfates.

The structure of boothite has not been refined, and thus the stereochemical details of the Cu^{2+} environment are not known, but it is a member of the melanterite group (Baur, 1964). Cyanochroite is isostructural with the minerals of the picromerite group (Carapezza & Riva di Sanseverino, 1970), all of which are natural analogues of the Tutton salt

Table 1. Cu^{2+} *oxysalt minerals: isolated polyhedra and finite-cluster structures*

Mineral	Formula	*a* (Å)	*b* (Å)	*c* (Å)	β (°)	Space group	Ref.	Fig.
Boothite	$[Cu(SO_4)(H_2O)_6](H_2O)$	–	–	–	–	–	–	–
Cyanochroite	$K_2[Cu(H_2O)_6(SO_4)_2]$	6.159 (5)	12.131 (7)	9.086 (4)	104.45 (5)	$P2_1/c$	(1)	–
Aubertite*	$[\{Cu(H_2O)_6\}\{Al(H_2O)_6\}(SO_4)_2]Cl(H_2O)_2$	6.282 (3)	13.192 (5)	6.260 (3)	94.70 (3)	$P\bar{1}$	(2)	–
Henmilite†	$Ca_2[Cu\{B(OH)_4\}_2(OH)_4]$	5.762 (1)	7.977 (1)	5.649 (1)	91.47 (1)	$P\bar{1}$	(3)	1

References: (1) Carapezza & Riva di Sanseverino (1968); (2) Ginderow & Cesbron (1979); (3) Nakai (1986).

* α = 91.85 (3), γ = 82.46 (3)°.
† α = 109.61 (1), γ = 83.69 (1)°.

Table 2. Cu^{2+} *oxysalt minerals: infinite chain structures*

Mineral	Formula	*a* (Å)	*b* (Å)	*c* (Å)	β (°)	Space group	Ref.	Linkage	Fig.
Eriochalcite	$[CuCl_2(H_2O)_2]$	7.38	8.04	3.72		$Pbmn$	(1)	$M{=}M$	2(*a*), 2(*b*)
Chloroxiphite	$Pb_3[CuCl_2(OH)_2O_2]$	10.458 (4)	5.759 (3)	6.693 (3)	97.79 (4)	$P2_1/m$	(2)	$M{=}M$	2(*c*)
Chalcanthite*	$[Cu(SO_4)(H_2O)_4](H_2O)$	6.105	10.72	5.949	107.3	$P\bar{1}$	(3)	$M{-}T$	3(*a*), 3(*b*)
Köhnkite	$Na_2[Cu(SO_4)_2(H_2O)_2]$	5.807 (1)	12.656 (2)	5.517 (1)	108.32 (1)	$P2_1/c$	(4)	$M{-}T$	3(*c*)
Cuprocopiapite	$[CuFe_4(SO_4)_6(OH)_2(H_2O)_{20}]$	7.34	18.19	7.28	101.5	$P\bar{1}$	–	$M{-}M{-}T$	3(*d*)
Caledonite†	$Pb_5[Cu_2(CO_3)(SO_4)_3(OH)_6]$	20.089 (7)	7.146 (3)	6.560 (5)		$Pmn2_1$	(5)	$M{=}M{-}T$	4(*a*), 4(*b*)
Linarite	$Pb[Cu(SO_4)(OH)_2]$	9.701 (2)	5.650 (2)	4.690 (2)	102.65 (2)	$P2_1/m$	(6)	$M{=}M{-}T$	4(*c*), 4(*d*)
Schmiederite	$Pb_2[Cu_2(SeO_3)(SeO_4)(OH)_4]$	9.922 (3)	5.712 (2)	9.396 (3)	101.96 (3)	$P2_1/m$	(6)	$M{=}M{-}T$	–
Tsumebite	$Pb_2[Cu(PO_4)(SO_4)(OH)]$	7.85	5.80	8.70	111.5	$P2_1/m$	(7)	$M{=}M{-}T$	–
Arsentsumebite	$Pb_2[Cu(SO_4)(AsO_4)(OH)]$	7.84	5.92	8.85	112.6	$P2_1/m$		$M{=}M{-}T$	
Fornacite	$Pb_2[Cu(CrO_4)(AsO_4)(OH)]$	8.101 (7)	5.892 (1)	17.547 (9)	110.00 (3)	$P2_1/c$	(8)	$M{=}M{-}T$	4(*e*), 4(*f*)
Molybdofornacite	$Pb_2[Cu(AsO_4)(MoO_4)(OH)]$	8.100 (5)	5.946 (3)	17.65 (1)	109.17 (5)	$P2_1/c$	–	$M{=}M{-}T$	–
Vauquelinite	$Pb_2[Cu(CrO_4)(PO_4)(OH)]$	13.754	5.806 (6)	9.563 (3)	94.56 (3)	$P2_1/n$	(9)	$M{=}M{-}T$	4(*e*), 4(*f*)
Chalconatronite	$Na_2[Cu(CO_3)_2(H_2O)_3]$	9.696 (2)	6.101 (2)	13.779 (3)	91.83 (2)	$P2_1/n$	(10)	$T{-}M{-}M{=}T$	5(*a*)
Chlorothionite	$K_2[Cu(SO_4)Cl_2]$	7.732 (2)	6.078 (1)	16.292 (3)		$Pnma$	(11)	$M{=}M{=}T$	5(*b*), 5(*c*)

References: (1) Harker (1936); (2) Finney *et al.* (1977); (3) Bacon & Curry (1962); (4) Hawthorne & Ferguson (1975); (5) Giacovazzo *et al.* (1973); (6) Effenberger (1987); (7) Nichols (1966); (8) Cocco *et al.* (1967); (9) Fanfani & Zanazzi (1968); (10) Mosset *et al.* (1978); (11) Giacovazzo *et al.* (1976).

* α = 82.4, γ = 102.6°.
† α = 93.85, γ = 99.33°.

Table 3. Cu^{2+} *oxysalt minerals: infinite sheet structures*

Mineral	Formula	*a* (Å)	*b* (Å)	*c* (Å)	β (°)	Space group	Ref.	*n*,*N*	Linkage	Fig.
Botallackite	$[Cu_2(OH)_3Cl]$	5.717 (1)	6.126 (1)	5.636 (1)	93.07 (1)	$P2_1/m$	(1)	2,0	$M{=}M$	6(*a*)
Posnjakite	$[Cu_4(SO_4)(OH)_6(H_2O)]$	10.578 (5)	6.345 (3)	7.863 (3)	117.98 (5)	Pa	(2)	4,1	$M{=}M{-}T$	6(*b*)
Wroewolfeite	$[Cu_4(SO_4)(OH)_6(H_2O)](H_2O)$	6.045 (1)	5.646 (1)	14.337 (2)	93.39 (1)	Pc	(3)	4,1	$M{=}M{-}T$	6(*c*)
Langite	$[Cu_4(SO_4)(OH)_6(H_2O)](H_2O)$	7.137 (3)	6.031 (5)	11.217 (1)	90.00 (1)	Pc	(4)	4,1	$M{=}M{-}T$	6(*d*)
Spangolite	$[Cu_6Al(SO_4)(OH)_{12}Cl](H_2O)_3$	8.256 (3)	*a*	14.367 (6)		$P31c$	(5)	7,1	$M{=}M{-}T$	7(*a*), 7(*b*)
Gerhardtite	$[Cu_2(NO_3)(OH)_3]$	6.087 (2)	13.813 (4)	5.597 (2)		$P2_12_12_1$	(6)	4,2	$M{=}M{-}T$	8(*a*)
Serpierite	$Ca[Cu_4(SO_4)_2(OH)_6](H_2O)_3$	22.186 (2)	6.250 (2)	21.853 (2)	113.36 (1)	$C2/c$	(7)	4,2	$M{=}M{-}T$	8(*c*)
Devilline	$Ca[Cu_4(SO_4)_2(OH)_6](H_2O)_3$	20.870 (2)	6.135 (2)	22.191 (3)	102.73 (2)	$P2_1/c$	(8)	4,2	$M{=}M{-}T$	8(*b*)
Campigliaite	$Mn[Cu_4(SO_4)_2(OH)_6](H_2O)_4$	21.725 (8)	6.118 (6)	11.233 (7)	100.40 (5)	$C2$	(9)	4,2	$M{=}M{-}T$	8(*d*)
Ktenasite	$Zn[(Cu,Zn)_4(SO_4)_2(OH)_6](H_2O)_6$	5.589 (1)	6.166 (1)	23.741 (7)	95.55 (1)	$P2_1/c$	(10)	4,2	$M{=}M{-}T$	8(*e*)
Bayldonite	$Pb[Cu_3(AsO_4)_2(OH)_2](H_2O)$	10.147 (2)	5.892 (1)	14.081 (2)	106.05 (1)	$C2/c$	(11)	4,2	$M{=}M{-}T$	9(*a*), 9(*b*)
Chalcophyllite	$[Cu_{18}Al_2(AsO_4)_4(OH)_{28}(H_2O)_{12}](SO_4)_3(H_2O)_{24}$	10.756 (2)	*a*	28.678 (4)		$R\bar{3}$	(12)	24,4	$M{=}M{-}T$	9(*c*), 9(*d*)
Roubaultite*	$[Cu_2(UO_2)_3(CO_3)_2O_2(OH)_3(H_2O)_4]$	7.767 (3)	6.924 (3)	7.850 (3)	90.89 (4)	$P\bar{1}$	(13)	–	$M{=}M{-}T$	10(*a*)
Turquoise†	$[CuAl_6(PO_4)_4(OH)_8(H_2O)_4]$	7.424 (4)	7.629 (3)	9.910 (4)	69.71 (4)	$P\bar{1}$	(14)	–	$M{=}M{-}T$	10(*b*), 10(*c*)
Likasite	$[Cu_3(NO_3)(OH)_5(H_2O)_2]$	5.830 (1)	6.775 (1)	21.711 (5)		$Pcmn$	(15)	–	$M{=}M{-}T$	10(*d*)
Sengierite	$[Cu_2(UO_2)_2(V_2O_8)(OH)_2(H_2O)_6]$	10.599 (5)	8.903 (4)	10.085 (9)	103.42 (6)	$P2_1/a$	(16)	–	$M{=}M{-}T$	
Cuproskłodowskite	$(H_3O)_2[Cu(UO_2)_2(SiO_3)_2(H_2O)_2]$	7.052 (5)	9.267 (8)	6.655 (5)	89.84 (5)	$P\bar{1}$	(17)	–	$M{-}T$	–
Metatorbernite‡	$[Cu(UO_2)_2(PO_4)_2(H_2O)_8$	6.969 (1)	*a*	17.306 (5)		$P4/n$	(18)		$M{-}T$	–
Osarizawaite	$Pb[CuAl_2(SO_4)_2(OH)_6]$	7.075 (1)	*a*	17.248 (2)		$R\bar{3}m$	(19)	–	$M{-}T{-}T$	11(*a*), 11(*b*)
Nissonite	$[Cu_2Mg_2(PO_4)_2(OH)_2(H_2O)_2](H_2O)$	22.523 (5)	5.015 (2)	10.506 (3)	99.62 (2)	$C2/c$	(20)	–	$M{=}M{-}T$	11(*c*), 11(*d*)

References: (1) Hawthorne (1985*c*); (2) Mellini & Merlino (1979); (3) Hawthorne & Groat (1985); (4) Gentsch & Weber (1984); (5) Hawthorne *et al.* (1992); (6) Bovio & Locchi (1982); (7) Sabelli & Zanazzi (1968); (8) Sabelli & Zanazzi (1972); (9) Sabelli (1982); (10) Mellini & Merlino (1978); (11) Ghose & Wan (1979); (12) Sabelli (1980); (13) Ginderow & Cesbron (1985); (14) Cid-Dresner (1965); (15) Effenberger (1986); (16) Piret *et al.* (1980); (17) Rosenzweig & Ryan (1975); (18) Ross *et al.* (1964); (19) Giuseppetti & Tadini (1980); (20) Groat & Hawthorne (1990).

* α = 92.16 (4), γ = 93.48 (4)°.
† α = 68.61 (3), γ = 65.08 (3)°.
‡ α = 109.23 (5), γ = 110.01 (7)°.

series $A_2^+M^{2+}(T^{6+}O_4)_2.6H_2O$, A^+ = Na, K, Rb, Cs; M^{2+} = Mg, Zn, Ni, Cu, Cd, Mn, V, Fe and Co (Brown & Chidambaram, 1969). Cyanochroite shows pronounced local distortion around Cu^{2+}, but the hydrogen-bonding system is flexible enough to accommodate the wide variation in polyhedral distortions shown by this structure type.

Finite-cluster structures

Henmilite is the only member of the finite-cluster group (Table 1), and the structure is shown in Fig. 1. An elongated $[Cu(OH)_6]$ octahedron links by corner sharing to two $[B(OH)_4]$ tetrahedra to give a $[Cu\{B(OH)_4\}_2(OH)_4]$ cluster graphically identical to

Table 4. Cu^{2+} *oxysalt minerals: infinite framework structures*

Mineral	Formula	*a* (Å)	*b* (Å)	*c* (Å)	*β* (°)	Space group	Ref.	Linkage*	Fig.
Atacamite	$[Cu_2Cl(OH)_3]$	6.030 (2)	6.865 (2)	9.120 (2)		*Pnma*	(1)	*M*=*M*	12(*a*), 12(*b*)
Paratacamite	$[Cu_2Cl(OH)_3]$	13.654 (5)	*a*	14.041 (6)		$R\bar{3}$	(2)	*M*=*M*	12(*a*), 12(*b*)
Bellingeritet	$[Cu_3(IO_3)_6(H_2O)_2]$	7.256 (2)	7.950 (2)	7.856 (2)	92.95 (2)	$P\bar{1}$	(3)	*M*=*M*	–
Salesite	$[Cu(IO_3)(OH)]$	10.794 (2)	6.708 (1)	4.781 (1)		*Pnma*	(4)	*M*=*M*	—
Mammothite	$Pb_6[Cu_4AlSbO_2(SO_4)_2(OH)_{16}Cl_4]$	18.93 (3)	7.33 (1)	11.35 (2)	112.4 (1)	*C*2/*m*	(5)	*M*—*M*=*M*—*T*	13(*a*), 13(*b*)
Bonattite	$[Cu(SO_4)(H_2O)_3]$	5.592 (5)	13.029 (9)	7.341 (6)	97.05 (9)	*Cc*	(6)	*M*—*T*	13(*c*), 13(*d*)
Poitevinite	$[(Cu,Fe,Zn)(SO_4)(H_2O)]$	7.176 (9)	7.426 (9)	7.635 (9)	116.15 (3)	*C*2/*c*	–	*M*—*M*—*T*	14(*a*)
Chalcomenite	$[Cu(SeO_3)(H_2O)_2]$	6.664 (5)	9.156 (5)	7.369 (5)		$P2_12_12_1$	(7)	*M*—*M*—*T*	14(*b*)
Teinite	$[Cu(TeO_3)(H_2O)_2]$	6.634 (4)	9.597 (5)	7.428 (4)		$P2_12_12_1$	(8)	*M*—*M*—*T*	
Bandylite	$[Cu\{B(OH)_4\}Cl]$	6.19	*a*	5.61		*P*4/*n*	(9)	*M*—*M*—*T*	14(*c*), 14(*d*)
Mixite	$Bi[Cu_6(AsO_4)_3(OH)_6(H_2O)_3]$	13.646 (2)	*a*	5.920 (1)		$P6_3/m$	(10)	*M*=*M*—*T* (*W*)	15(*a*), 16(*a*)
Agardite-(Y)	$(Y,REE)[Cu_6(AsO_4)_3(OH)_6(H_2O)_3]$	13.583 (2)	*a*	5.895 (1)		$P6_3/m$	(11)	*M*=*M*—*T* (*W*)	–
Goudeyite	$(Y,Al)[Cu_6(AsO_4)_3(OH)_6(H_2O)_3]$	13.472 (1)	*a*	5.902 (4)		$P6_3/m$	–	*M*=*M*—*T* (*W*)	–
Petersite-(Y)	$(Y,REE)[Cu_6(PO_4)_3(OH)_6(H_2O)_3]$	13.288 (5)	*a*	5.877 (5)		$P6_3/m$	–	*M*=*M*—*T* (*W*)	–
Conichalcite	$Ca[Cu(AsO_4)(OH)]$	7.40	9.21	5.84		$P2_12_12_1$	(12)	*M*=*M*—*T* (*W*)	15(*b*), 16(*b*)
Mottramite	$Pb[Cu(VO_4)(OH)]$	7.682	9.278	6.034		*Pnam*	–	*M*=*M*—*T* (*W*)	–
Calciovolborthite	$Ca[Cu(VO_4)(OH)]$	7.45	9.26	5.91		*Pnam*	–	*M*=*M*—*T* (*W*)	–
Euchroite	$[Cu_2(AsO_4)(OH)(H_2O)_3]$	10.056 (2)	10.506 (2)	6.103 (2)		$P2_12_12_1$	(13)	*M*=*M*—*T* (*W*)	15(*c*), 16(*c*), 17(*a*)
Antlerite	$[Cu_3(SO_4)(OH)_4]$	8.244 (2)	6.043 (1)	11.987 (3)		*Pnma*	(14)	*M*=*M*—*T* (*W*)	15(*d*), 16(*d*), 17(*b*)
Chalcocyanite	$[Cu(SO_4)]$	8.409 (1)	6.709 (1)	4.833 (1)		*Pnma*	(15)	*M*=*M*—*T*	18(*a*), 18(*b*)
Trippkeite	$[Cu(As_2O_4)]$	8.592 (4)	*a*	5.573 (4)		$P4_2mbc$	(16)	*M*=*M*—*T*	18(*c*), 18(*d*)
Lindgrenite	$[Cu_3(MoO_4)_2(OH)_2]$	5.394 (1)	14.023 (3)	5.608 (1)	98.50 (1)	$P2_1/n$	(17)	*M*=*M*—*T*	18(*e*), 18(*f*)
Cornubite‡	$[Cu_5(AsO_4)_2(OH)_4]$	6.121 (1)	6.251 (1)	6.790 (1)	111.30 (1)	$P\bar{1}$	(18)	*M*=*M*—*T*	20(*b*)
Pseudomalachite	$[Cu_5(PO_4)_2(OH)_4(H_2O)]$	4.473 (1)	5.747 (1)	17.032 (3)	91.04 (1)	$P2_1/c$	(19)	*M*=*M*—*T*	19(*a*)
Reichenbachite	$[Cu_5(PO_4)_2(OH)_4(H_2O)]$	9.186 (2)	10.684 (2)	4.461 (1)	92.31 (1)	$P2_1/a$	(20)	*M*=*M*—*T*	19(*b*)
Ludjibaite§ [QPM]	$[Cu_5(PO_4)_2(OH)_4(H_2O)]$	4.446 (3)	5.871 (4)	8.680 (7)	90.3 (2)	$P\bar{1}$	(21)	*M*=*M*—*T*	19(*c*), 20(*a*)
Mcbirneyite	$[Cu_3(VO_4)_2]$	6.249 (1)	7.994 (1)	6.378 (1)	111.49 (1)	$P2_1/c$	(22)	*M*=*M*—*T*	21(*a*), 21(*b*)
Malachite	$[Cu_2(CO_3)(OH)_2]$	9.502	11.974	3.240	98.75	$P2_1/a$	(23)	*M*—*M*=*M*—*T* (*W*)	16(*f*)
Arthurite	$[CuFe_2^{3+}(AsO_4)_2(OH)_2(H_2O)_4]$	10.189 (2)	9.649 (2)	5.598 (1)	92.16 (2)	$P2_1/c$	(24)	*M*—*M*=*M*—*T*	22(*a*)
Lammerite	$[Cu_3(AsO_4)_2]$	5.079 (1)	11.611 (2)	5.394 (1)	111.72 (2)	$P2_1/a$	(25)	*M*—*M*=*M*—*T*	22(*b*), 22(*c*), 22(*d*)
Hentschelite	$[CuFe_2(PO_4)_2(OH)_2]$	6.984 (3)	7.786 (3)	7.266 (3)	117.68 (2)	$P2_1/n$	(26)	*M*—*M*=*M*—*T*	22(*e*)
Ramsbeckite	$[(Cu,Zn)_{15}(SO_4)_4(OH)_{22}](H_2O)_6$	16.088 (4)	15.576 (4)	7.102 (2)	90.22 (2)	$P2_1/a$	(27)	*M*—*M*=*M*—*T*	22(*f*)
Cornetite	$[Cu_3(PO_4)(OH)_3]$	10.854 (1)	14.053 (3)	7.086 (2)		*Pbca*	(28)	*M*—*M*=*M*—*T*	23(*a*), 23(*b*)
Volborthite	$[Cu_3(V_2O_7)(OH)_2](H_2O)_2$	10.610 (2)	5.866 (1)	7.208 (1)	95.04 (2)	*C*2/*m*	(29)	*M*=*M*—*T*—*T*	24(*a*)
Papagoite	$[CaCuAl(Si_2O_6)(OH)_3]$	12.926 (3)	11.496 (3)	4.696 (1)	100.81 (2)	*C*2/*m*	(30)	*M*=*M*—*T*—*T* (*W*)	15(*e*), 16(*e*)
Dioptase	$[Cu_6Si_6O_{18}(H_2O)_6]$	14.566	*a*	7.778		*R*3	(31)	*M*=*M*—*T*—*T*	24(*b*)
Shattuckite	$[Cu_5(SiO_3)_4(OH)_2]$	9.885 (1)	19.832 (2)	5.383 (1)		*Pcab*	(32)	*M*=*M*—*T*—*T*	25(*a*)
Plancheite	$[Cu_8(Si_8O_{22})(OH)_4(H_2O)]$	19.043 (3)	20.129 (5)	5.269 (1)		*Pcnb*	(32)	*M*=*M*—*T*—*T*	25(*b*), 25(*c*)
Veszelyite	$[(Cu,Zn)_2Zn(PO_4)(OH)_3(H_2O)_2]$	9.828 (3)	10.224 (3)	7.532 (2)	103.18 (2)	$P2_1/a$	(33)	*M*=*M*—*T*—*T*	26(*a*), 26(*b*)
Kipushite	$[(Cu,Zn)_5Zn(PO_4)_2(OH)_6(H_2O)]$	12.197 (2)	9.156 (2)	10.667 (2)	96.77 (2)	$P2_1/c$	(34)	*M*=*M*—*T*—*T*	

References: (1) Parise & Hyde (1986); (2) Fleet (1975); (3) Ghose & Wan (1974); (4) Ghose & Wan (1978); (5) Effenberger (1985*a*); (6) Zahrobsky & Baur (1968); (7) Asai & Kiriyama (1973); (8) Effenberger (1977); (9) Collins (1951); (10) Mereiter & Preisinger (1986); (11) Aruga & Nakai (1985); (12) Qurashi & Barnes (1963); (13) Eby & Hawthorne (1989*a*); (14) Hawthorne *et al.* (1989); (15) Wildner & Giester (1988); (16) Pertlik (1975); (17) Hawthorne & Eby (1985); (18) Tillmanns *et al.* (1985); (19) Shoemaker *et al.* (1977); (20) Anderson *et al.* (1977); (21) Shoemaker *et al.* (1981), Piret & Deliens (1988); (22) Shannon & Calvo (1972); (23) Zigan *et al.* (1977); (24) Keller & Hess (1978); (25) Hawthorne (1986*b*); (26) Sieber *et al.* (1984); (27) Effenberger (1988); (28) Eby & Hawthorne (1989*b*); (29) Basso *et al.* (1988); (30) Groat & Hawthorne (1987); (31) Ribbe *et al.* (1977); (32) Evans & Mrose (1977); (33) Ghose *et al.* (1974); (34) Piret *et al.* (1985).

* (*W*) = wallpaper structure.
† α = 105.10 (2), γ = 96.95 (2)°.
‡ α = 92.93 (1), γ = 107.47 (1)°.
§ α = 103.9 (2), γ = 93.2 (2)°.

Table 5. Cu^{2+} *oxysalt minerals with* Cu^{2+} *in non-octahedral coordinations*

Mineral	Formula	*a* (Å)	*b* (Å)	*c* (Å)	*β* (°)	Space group	Ref.	Linkage*	[CN]	Fig.
Lyonsite	$[Cu_3Fe_4(VO_4)_6]$	10.296 (1)	17.207 (2)	4.910 (1)		*Pmcn*	(1)	*M*=*M*—*T*—*M*=*M*	5	27(*a*), 27(*b*)
Ziesite	$[Cu_2(V_2O_7)]$	7.685 (5)	8.007 (3)	10.09 (2)	110.27 (5)	*C*2/*c*	(2)	*M*—*M*—*T*—*T*	5	28(*a*)
Blossite	$[Cu_2(V_2O_7)]$	20.65 (5)	8.383 (7)	6.44 (1)		*Fdd*2	(3)	*M*—*M*—*T*—*T*	5	–
Kinoite	$Ca_2[Cu_2(Si_3O_8)(OH)_4]$	6.991 (2)	12.890 (3)	5.654 (2)	96.18 (3)	$P2_1/m$	(4)	*M*—*M*—*T*—*T*	5	28(*b*), 28(*c*)
Cuprorivaite	$Ca[Cu(Si_4O_{10})]$	7.30 (1)	*a*	15.12 (2)		*P*4/*nnc*	(5)	*M*—*M*—*T*	4	29(*a*), 29(*b*)
Azurite	$[Cu_3(CO_3)_2(OH)_2]$	5.011 (1)	5.849 (1)	10.345 (2)	92.43 (3)	$P2_1/c$	(6)	*M*—*M*—*T*	4,6	30(*a*), 30(*b*)
Stringhamite	$Ca[Cu(SiO_4)](H_2O)$	5.030 (2)	16.135 (3)	5.343 (1)	102.96 (1)	$P2_1/c$	(7)	*M*—*T*	4,6	30(*c*), 30(*d*)
Olivenite	$[Cu_2(AsO_4)(OH)]$	8.615 (5)	8.240 (5)	5.953 (4)	90.0 (1)	$P2_1/n$	(8)	*M*=*M*—*T* (*W*)	5,6	15(*f*), 16(*b*)
Libethenite	$[Cu_2(PO_4)(OH)]$	8.062 (5)	8.384 (4)	5.881 (2)		*Pnnm*	(9)	*M*=*M*—*T* (*W*)	5,6	15(*f*), 16(*b*)
Callaghanite	$[Cu_2Mg_2(CO_3)(OH)_6(H_2O)_2]$	10.006 (1)	11.752 (1)	8.213 (1)	107.38 (2)	*C*2/*c*	(10)	*M*=*M*—*T*	5,6	–
Stranskiite†	$[Zn_2Cu(AsO_4)_2]$	5.092 (2)	6.695 (2)	5.304 (2)	112.09 (2)	$P\bar{1}$	(11)	*M*=*M*—*T*	5,6	31(*a*), 31(*b*)
Stoiberite	$[Cu_5(V_2O_{10})]$	8.393 (2)	6.065 (1)	16.156 (3)	108.09 (2)	$P2_1/c$	(12)	*M*=*M*—*T*	5,6	31(*c*), 31(*d*)
Fingerite‡	$[Cu_{11}O_2(VO_4)_6]$	8.158 (1)	8.269 (1)	8.044 (1)	91.39 (1)	$P\bar{1}$	(13)	*M*=*M*—*T*	5,6	32(*a*), 32(*b*)
Dolerophanite	$[Cu_2O(SO_4)]$	9.370 (1)	6.319 (1)	7.639 (1)	122.34 (1)	*C*2/*m*	(14)	*M*=*M*—*T*	5,6	32(*c*), 32(*d*)
Clinoclase	$[Cu_3(AsO_4)(OH)_3]$	7.257 (2)	6.457 (2)	12.378 (3)	99.51 (2)	$P2_1/c$	(15)	*M*=*M*—*T*	5,6	

References: (1) Hughes *et al.* (1987); (2) Mercurio-Lavaud & Frit (1973); (3) Calvo & Faggiani (1975); (4) Laughon (1971); (5) Pabst (1959); (6) Zigan & Schuster (1972); (7) Hawthorne (1985*d*); (8) Toman (1977); (9) Corsden (1978); (10) Brunton (1973); (11) Keller *et al.* (1979); (12) Shannon & Calvo (1973); (13) Finger (1985); (14) Effenberger (1985*b*); (15) Eby & Hawthorne (1990).

* (*W*) = wallpaper structure.
† α = 110.16 (2), γ = 86.74 (2)°.
‡ α = 107.14 (1), γ = 106.44 (1)°.

the $[M(TO_4)_2(H_2O)_4]$ cluster found in blödite and related structures (Hawthorne, 1985*b*). These clusters are linked by [8]-coordinate Ca and by hydrogen bonds.

Infinite chain structures

Structures based on infinite chains are given in Table 2. Within this group, the chains are further divided on the basis of their internal connectivity.

M=M chains

In eriochalcite, $[Cu^{2+}Cl_4(H_2O)_2]$ octahedra link into chains by sharing edges (Fig. 2*a*), each octahedron being flanked by two others in a *trans* arrangement. The chains are linked by hydrogen bonding between the apical (H_2O) groups of one chain and the meridional Cl atoms of adjacent chains (Fig. 2*b*).

M≡M chains

In chloroxiphite, $(Cu^{2+}O_4Cl_2)$ octahedra polymerize by sharing faces (in a *trans* configuration) to form $[M\varphi_3]$ chains along [010] (Fig. 2*c*). The chains are cross-linked by an array of [7]-coordinate Pb^{2+} to give a fairly isodesmic structure (Fig. 2*d*).

M—T chains

The chalcanthite structure (Figs. 3*a*, 3*b*) consists of $[M(TO_4)\varphi_4]$ chains extending along [110], and cross-linked by a hydrogen-bonding network involving one (H_2O) group that bonds to no cations other than hydrogen. Kröhnkite (Fig. 3*c*) has $[M(TO_4)\varphi_2]$ chains that extend along [001]; these are cross-linked by [7]-coordinate Na and by hydrogen bonds associated with the (H_2O) groups. Both of these minerals are isostructural with non-Cu^{2+} species or synthetic compounds. Chalcanthite is isostructural with $Mg(CrO_4).5H_2O$ (Baur & Rolin, 1972). Kröhnkite is isostructural with a series of Ca minerals, $CaM^{2+}(AsO_4).2H_2O$, M^{2+} = Mg, Co, Mn and Ni, although there are no other natural Na analogues of kröhnkite itself.

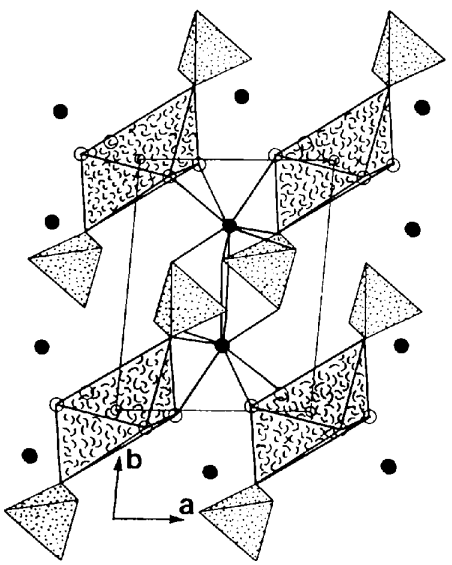

Fig. 1. Finite-cluster copper minerals: henmilite, an $[M(TO_4)_2\varphi_4]$ structure; ($Cu\varphi_6$) octahedra are curl shaded, ($B\varphi_4$) tetrahedra are dot shaded, and most linking Ca—φ bonds are omitted for clarity.

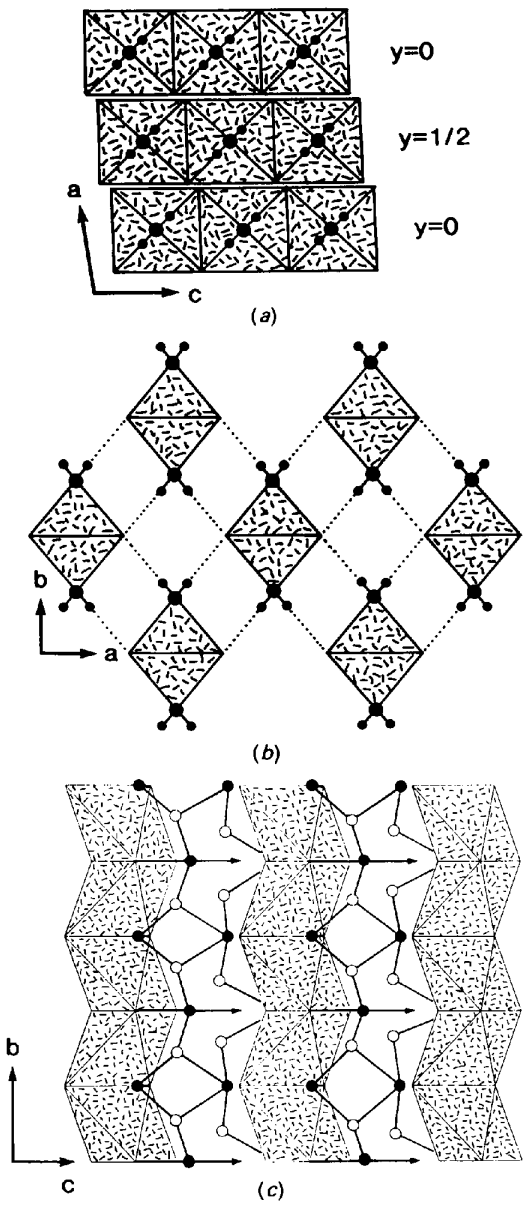

Fig. 2. Infinite chain copper minerals: (*a*), (*b*) eriochalcite, with edge-sharing [$Cu\varphi_4$] octahedral chains; (*c*) chloroxiphite, with face-sharing [$Cu\varphi_3$] octahedral chains; octahedra are dash shaded, long Pb—φ bonds in chloroxiphite are omitted for clarity.

M—M—T chains

Cuprocopiapite has not been studied, but it is isostructural with copiapite (Süsse, 1972; Fanfani, Nunzi, Zanazzi & Zanzari, 1973). The structure has complex *M—M—T* chains (Fig. 3*d*), consisting of $[Mg_2(SO_4)_2O_2(OH)(H_2O)_4]$ clusters linked by (SO_4) tetrahedra. This $[M_2(TO_4)_2\varphi_7]$ cluster is the basis of an extensive hierarchy of structures (Hawthorne, 1979). These chains are cross-linked by a hydrogen-bonding network that involves isolated $[Cu(H_2O)_6]$ octahedra.

M=M—T chains

This is the largest group within the chain structures. The basic unit is the *trans* edge-sharing $[Cu_2\varphi_8]$ chain, and the different chains are produced by decorating this basic unit with differently connected tetrahedra. The simplest chain is found in caledonite (Fig. 4*a*). Each (SO_4) tetrahedron shares one corner with the chain, connecting to one anion of the shared edge between adjacent octahedra; the tetrahedra take up a staggered arrangement along the chain. These chains are then linked together *via* $Pb^{2+}—\varphi$ and hydrogen bonds that also involve a carbonate group and an additional sulfate group (Fig. 4*b*).

In linarite (Fig. 4*c*), the flanking tetrahedra again assume a staggered arrangement, but in this case, each tetrahedron shares two vertices with the chain and links across the apical anions of the adjoining octahedra. The chains are cross-linked by [10]- and [11]-coordinate Pb^{2+} and by hydrogen bonds (Fig. 4*d*). The chains in schmiederite are very similar, except that half of the tetrahedra are replaced by carbonate groups, and again the cross-linkage is provided by $Pb^{2+}—\varphi$ and hydrogen bonds.

Fornacite and vauquelinite have the most highly connected chains of this basic type (Fig. 4*e*). Adjacent apical vertices of the edge-sharing octahedra are linked by tetrahedra (as in the linarite-type chains). In addition to this, one anion of each shared octahedral edge links to another tetrahedron (as in the caledonite-like chain), each different type of tetrahedron lying on opposite sides of the chain. These complex chains are then cross-linked by $Pb^{2+}—\varphi$ and hydrogen bonds. Fornacite and vauquelinite are not isostructural, but their structures are extremely similar (Fig. 4*f*).

T—M—M=T chains

In chalconatronite, the octahedra link *via* corners to form a very convoluted $[M_2\varphi_{10}]$ chain (Fig. 5*a*) that extends along [010]. Two distinct carbonate triangles decorate the length of the chain, playing graphically distinct roles, and the resulting chains are cross-linked by Na atoms and hydrogen bonding.

M=M=T chains

As emphasized by Giacovazzo, Scandale & Scordari (1976), chlorothionite has a most unusual chain of edge-sharing octahedra and tetrahedra

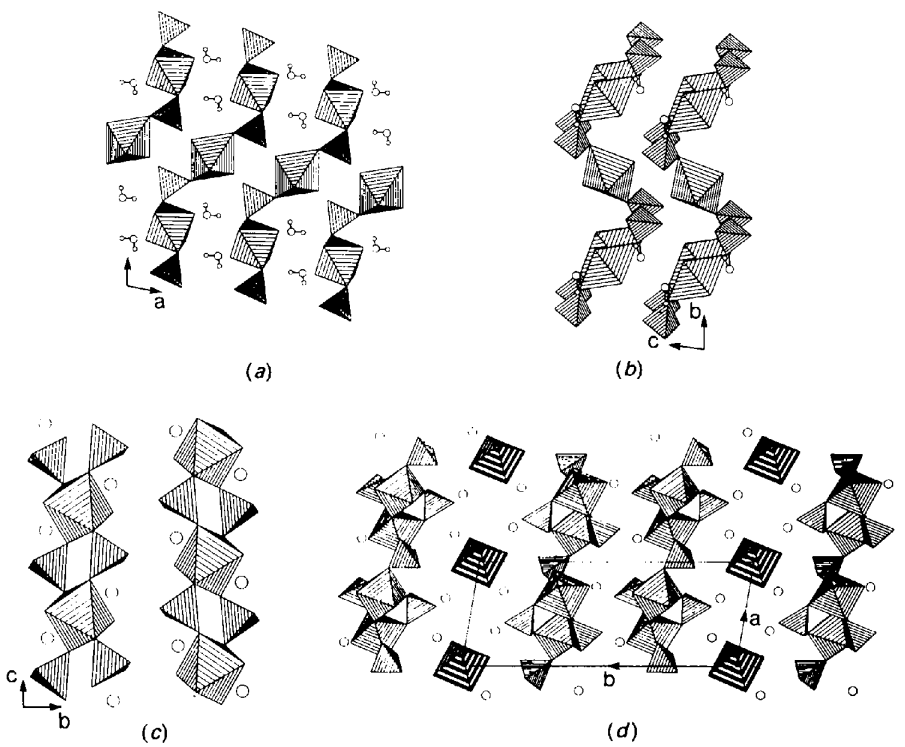

Fig. 3. Infinite chain copper minerals: (*a*), (*b*) chalcanthite, with corner-sharing $[Cu(SO_4)(H_2O)_4]$ octahedral–tetrahedral chains; (*c*) kröhnkite, with corner-sharing $[Cu(SO_4)_2(H_2O)_2]$ chains; (*d*) copiapite (cuprocopiapite), with complex corner-sharing $[Fe_4(SO_4)_6(OH)_2(H_2O)_n]$ chains; linking $[Cu(H_2O)_6]$ octahedra are shown in stripes. In all structures, bonds between structural units and between interstitial species and structural units are omitted for clarity.

(Figs. 5*b*, 5*c*). The octahedra share edges, but in an octahedron, the shared edges are *cis*, giving a zigzag octahedral chain. The tetrahedra decorate the periphery of the chain, sharing edges with the octahedra across the O—O meridional edge. These unusual chains are cross-linked by K—Cl and K—O bonds.

Infinite sheet structures

The minerals in this class are given in Table 3. They are all characterized by strongly bonded sheets of polyhedra, linked in the third dimension by weaker bonds usually involving highly coordinated alkali and alkaline-earth cations, together with hydrogen bonding. As briefly discussed by Hawthorne (1985*c*), many of these structures are based on a sheet of edge-sharing octahedra (not all of which are necessarily occupied by cations) that may be further decorated by the attachment of other polyhedra to one or both sides of the sheet. They may be written as $^{[6]}M_nT_N\varphi_{2n-N}$, in which T represents a complex anion [OH, H_2O, $(T\varphi_4)$, $(T\varphi_3)$]; the members of this series are given in Table 3.

M=*M sheets*

When $N=0$, there are no polyhedral decorations to the basic sheet, and we have the structure of botallackite, shown in Fig. 6(*a*). The sheets are linked together by hydrogen bonding from the hydroxyl donors of one sheet to the Cl acceptors of the adjacent sheets.

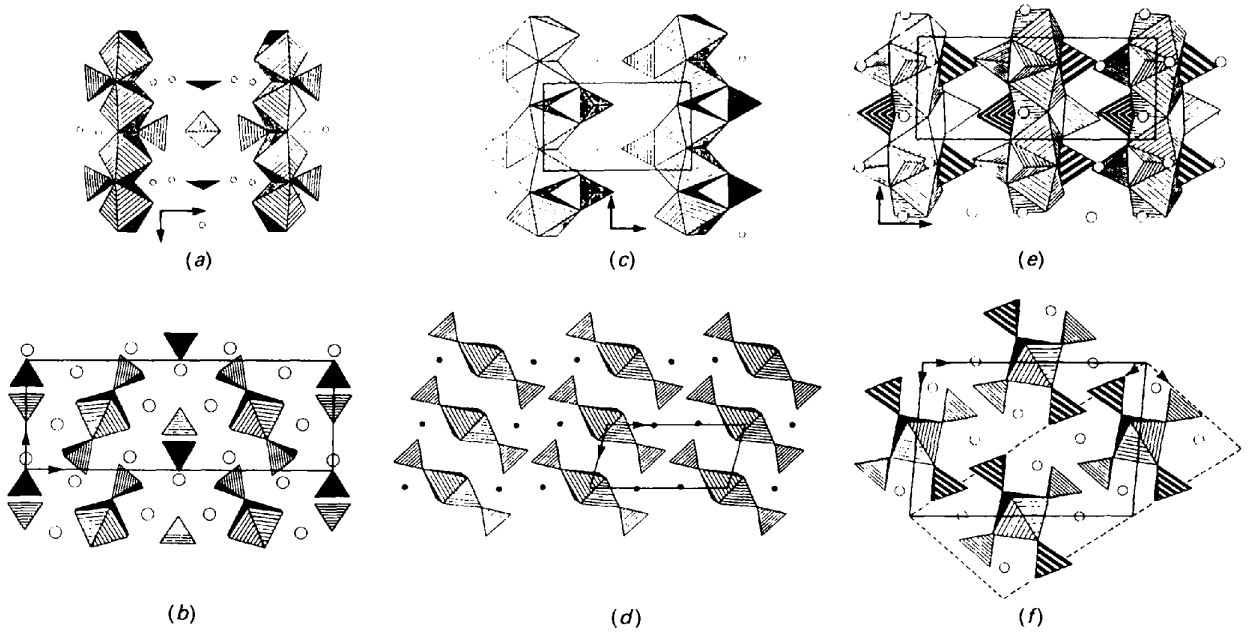

Fig. 4. Infinite chain copper minerals with edge sharing between octahedra in heteropolyhedral chains: (*a*), (*b*) caledonite, with $[Cu_2(SO_4)_2(OH)_6]$ chains, and (CO_3) triangles shown in black; (*c*), (*d*) linarite, with $[Cu(SO_4)(OH)_2]$ chains; (*e*), (*f*) fornacite and vauquelinite (dashed cell), with $[Cu(CrO_4)(AsO_4)(OH)]$ chains; (CrO_4) tetrahedra are shown in stripes. All bonds between interstitial species and structural units are omitted for clarity.

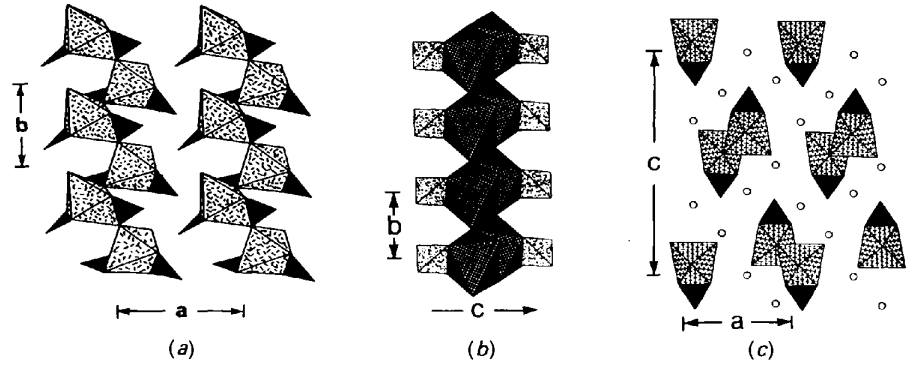

Fig. 5. Infinite chain copper minerals with edge sharing between octahedra and tetrahedra (dotted) or triangles (black): (*a*) chalconatronite, with $[Cu(CO_3)_2(H_2O)_3]$ edge-sharing chains; (*b*), (*c*) chlorothionite, with $[Cu(SO_4)Cl_2]$ edge-sharing chains. All bonds between interstitial species and structural units are omitted for clarity.

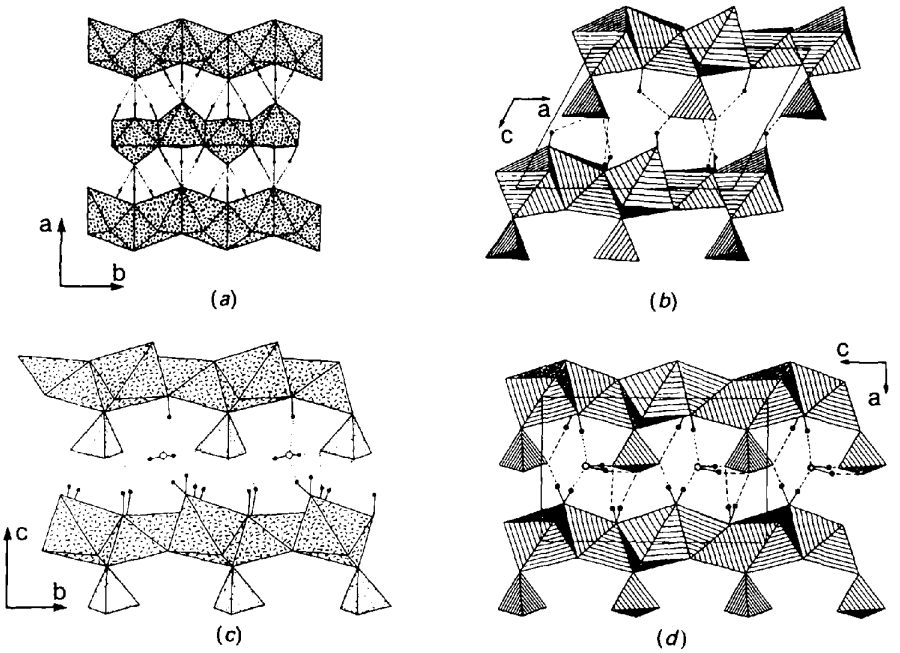

Fig. 6. Infinite sheet copper minerals with edge-sharing $[Cu\varphi_2]$ sheets undecorated or decorated on one side: (*a*) botallackite, with an undecorated $[Cu_2(OH)_3Cl]$ sheet; (*b*) posnjakite, with a decorated $[Cu_4(SO_4)(OH)_6(H_2O)]$ sheet; (*c*) wroewolfeite, with a sheet similar to (*b*); (*d*) langite, with a similar sheet to (*b*); note that (*c*) and (*d*) both have interstitial (H_2O) whereas (*b*) does not. Hydrogen bonds are denoted by broken lines.

M=M—T sheets

This is the largest of the subgroups in the sheet structure class, and it can be divided into two parts.

$^{[6]}M_nT_N\varphi_{2n-N}$ *structures*. For $N=1$, the structures have one side of the octahedral sheet decorated by (sulfate) tetrahedra. The simplest structure (Fig. 6*b*) is posnjakite, $n=4$ and $N=1$, with the general formula $M_4T_1\varphi_7$ $[Cu_4(SO_4)(OH)_6(H_2O)]$. The sheets are repeated by simple translation, and linked together solely by hydrogen bonding. Wroewolfeite and langite also have $n=4$ and $N=1$; their sheets are graphically identical to the sheet in posnjakite. However, both structures have an interstitial (H_2O) group that is a part of the interlayer hydrogen-bonded network linking the sheets together (Figs. 6*c*, 6*d*).

Spangolite (Fig. 7) has an edge-sharing sheet of Cu^{2+} and Al in the ratio 6:1; thus $n=7$. There is one sulfate tetrahedron per seven octahedrally coordinated cations, and spangolite has the general form $M_7T\varphi_{13}$; the formula $Cu_6Al(SO_4)(OH)_{12}Cl$ fits this exactly. The sheets are linked solely by hydrogen bonding, with three interlayer (H_2O) groups.

For $N=2$, the tetrahedra occur on both sides of the octahedral sheets. The simplest structure is

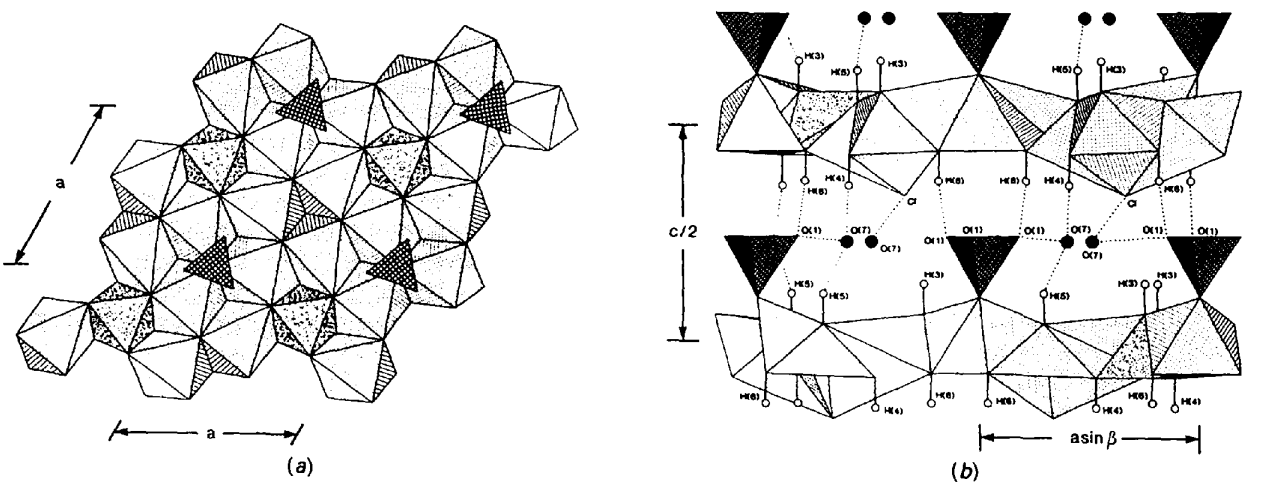

Fig. 7. Infinite sheet copper minerals with sheets decorated on one side; spangolite: (*a*) the constitution of the $[M_7T\varphi_{13}]$ sheet; (*b*) adjacent sheets showing the one-sided decoration by (SO_4) tetrahedra and the linking hydrogen-bonded network; ($Al\varphi_6$) octahedra are denoted by random dots.

gerhardtite, in which (NO_3) triangles flank both sides of a close-packed octahedral sheet; linkage is provided by hydrogen bonds from the octahedral vertices to the corners of the opposing (NO_3) groups (Fig. 8*a*). There is also a synthetic polymorph of gerhardtite which has graphically identical sheets (Effenberger, 1983) that stack differently, giving rise to the difference in symmetry.

The other $N = 2$ structures, serpierite, devilline, campigliaite and ktenasite, can be considered as insertion structures, whereby different structural units are incorporated between the basic $[Cu_4(SO_4)(OH)_6]$ sheets. Devilline and serpierite are the simplest $N = 2$ structures. Different intersheet linkage (Sabelli & Zanazzi, 1968) gives rise to two different structures from graphically identical structural units. In both minerals, the sheets are cross-linked by [7]-coordinate Ca atoms (Figs. 8*b*, 8*c*), together with (different) hydrogen-bonded networks that involve intersheet (H_2O) groups.

In campigliaite, the basic $[Cu_4(SO_4)(OH)_6]$ sheets are cross-linked by $[MnO_2(H_2O)_4]$ octahedra (Fig. 8*d*). Each $[MnO_2(H_2O)_4]$ octahedron shares two oxygens with sulfate groups from one sheet, and the remaining coordinating (H_2O) groups hydrogen bond (primarily) to the adjacent sheet to provide the (weak) intersheet linkage. Ktenasite takes this process one step further. The basic sheets are cross-linked by a hydrogen-bonded network that involves $[Zn(H_2O)_6]$ octahedra at an intersheet position (Fig. 8*e*).

The bayldonite and chalcophyllite structures are significantly different from the sheet structures so far discussed, the tetrahedra associated with the

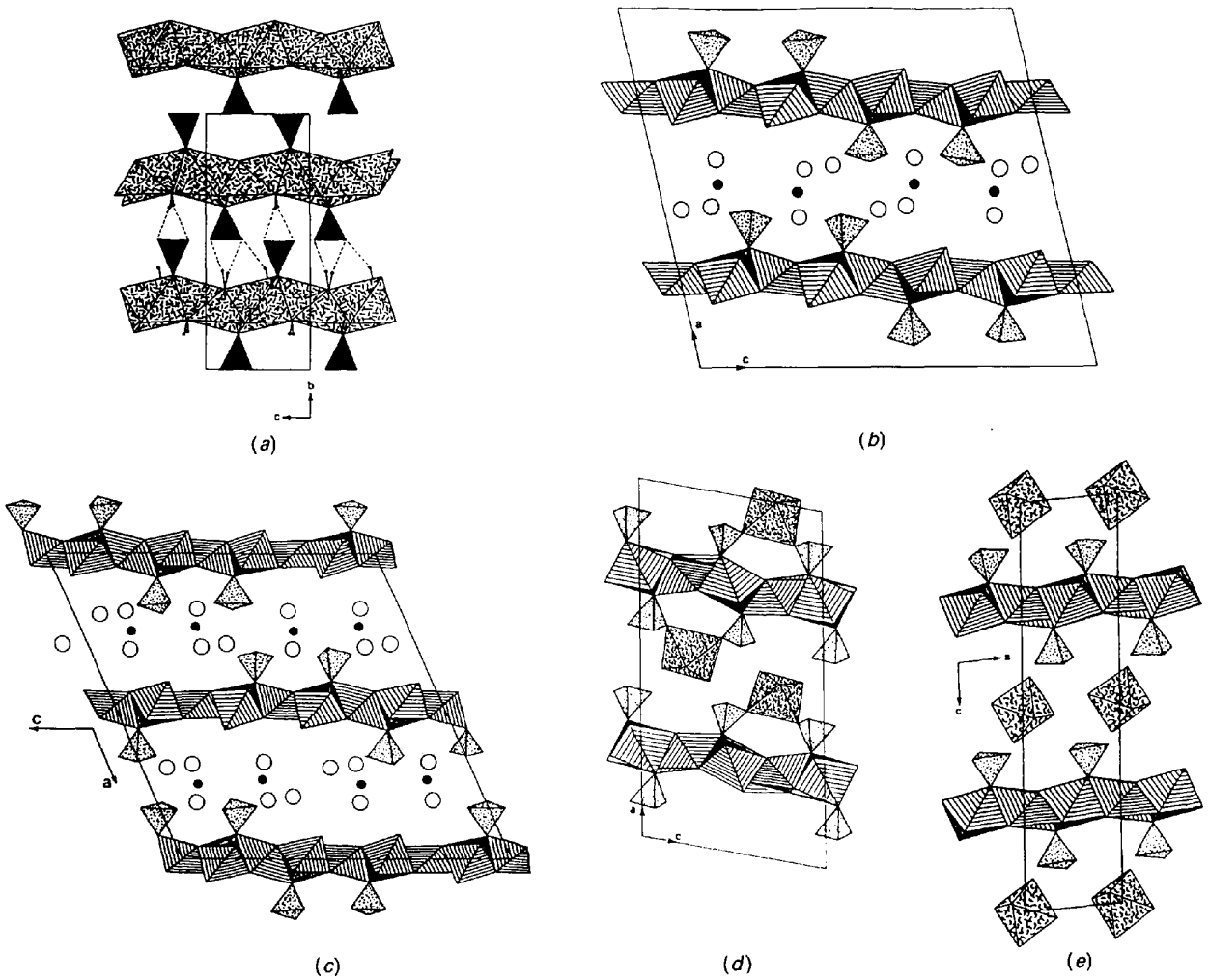

Fig. 8. Infinite sheet copper minerals with edge-sharing $[Cu\varphi_2]$ sheets decorated on both sides: (*a*) gerhardtite, with a $[Cu_2(NO_3)(OH)_3]$ sheet in which the triangular (NO_3) groups are shown as black triangles; (*b*) devilline, with $[Cu_4(SO_4)_2(OH)_6]$ sheets; (*c*) serpierite, with the same sheets as (*b*); (*d*) campigliaite, with the same sheets as (*b*); (*e*) ktenasite, with $[(Cu,Zn)_4(SO_4)_2(OH)_6]$ sheets graphically the same as in (*b*). Black circles are interstitial cations, hollow circles are interstitial (H_2O) groups; hydrogen bonds are omitted for clarity or through ignorance.

octahedral sheet sharing three vertices (rather than one) with the octahedra of the sheet; the resultant general formula is $[M_nT_n\varphi_{2n-3N}]$. For bayldonite, the octahedral sheet is only $\frac{3}{4}$ occupied (Fig. 9*a*); hence $n = 4$ ($Cu_3\square$) and $N = 2$, with $\varphi_{2n-3N} = \varphi_2$, giving the general sheet formula $[(Cu_3\square)(AsO_4)_2(OH)_2]$. These sheets are linked by [8]-coordinate Pb and by a hydrogen-bonding network involving the interlayer (H_2O) group (Fig. 9*b*). In chalcophyllite, the octahedral sheets (Fig. 9*c*) are partly occupied by Cu^{2+} and Al, and opposing each vacant octahedral site is an arsenate group which shares a face with the vacant octahedron. The sheet formula can thus be written as $M_{24}T_4\varphi_{2\times24-3\times4} = [(Cu_{18}Al_2\square_4)(AsO_4)_4\varphi_{36}]$. Cross-linkage involves $(SO_4)^{2-}$ oxyanions that are incorporated into a complex hydrogen-bonding network that also involves both sheet and intersheet (H_2O) groups (Fig. 9*d*).

Miscellaneous edge-sharing sheets. In roubaultite, rutile-like $[M\varphi_4]$ chains of ($Cu\varphi_6$) octahedra and edge-sharing chains of pentagonal ($U\varphi_7$) and hexagonal ($U\varphi_8$) dipyramids and carbonate groups extend along [010], and share corners to form sheets (Fig. 10*a*) parallel to (101). These sheets are linked solely by hydrogen-bonding involving the (OH) and (H_2O) groups of the ($Cu\varphi_6$) groups. In turquoise, an $[AlCuAl\varphi_{14}]$ linear edge-sharing trimer links by corner sharing to a $[Cu_2(PO_4)_2\varphi_8]$ octahedral/tetrahedral cluster to form a thick sheet parallel to (001) (Fig. 10*b*). These layers stack along [001] (Fig. 10*c*), and interlayer linkage is through a hydrogen-bonding network.

Likasite consists of interlocking orthogonal edge-sharing octahedral chains that form a three-layer octahedral sheet (Fig. 10*d*), resembling a slice from the atacamite structure. Flanking the external chains are (NO_3) triangles that link vertices of adjacent octahedra in these chains, with the third vertex acting as a hydrogen-bond acceptor for the (OH) anions in the adjacent sheet.

The remaining minerals, sengierite and cuprosklodowskite, are structures in which ($Cu\varphi_6$) octahedra do not participate in the structural unit, but act as interstitial components.

M—T sheet structures

Metatorbernite consists of strongly bonded layers of corner-sharing (PO_4) tetrahedra and ($U\varphi_6$) octahedra that are cross-linked by ($Cu\varphi_6$) octahedra through their long apical bonds.

M—M—T sheet structures

Osarizawaite is a member of the alunite group (Figs. 11*a*, 11*b*). According to the structure refinement (Giuseppetti & Tadini, 1980), ($CuAl_2$) is

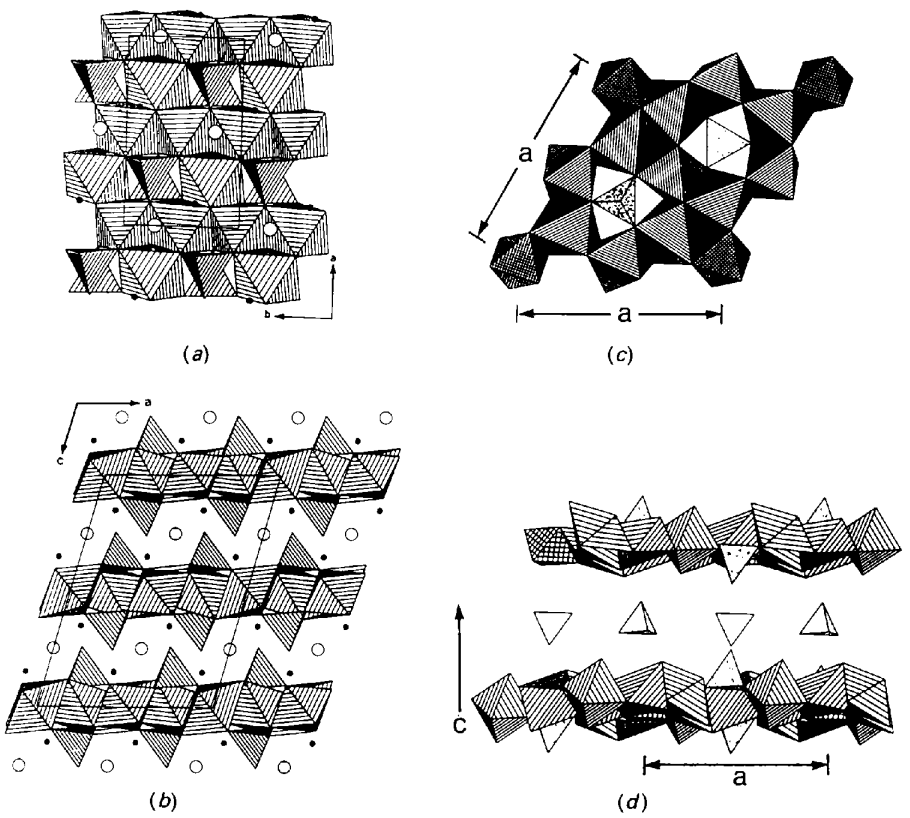

Fig. 9. Infinite sheet copper minerals with edge-sharing $[(Cu_3\square)\varphi_2]$ sheets decorated by tetrahedra: (*a*), (*b*) bayldonite, with a $[(Cu_3)(AsO_4)_2(OH)_2]$ sheet; (*c*), (*d*) chalcophyllite, with a $[Cu_{18}Al_2(AsO_4)_4(OH)_{24}(H_2O)_{12}]$ sheet in which ($Cu\varphi_6$) octahedra are lined and ($Al\varphi_6$) are cross-hatched.

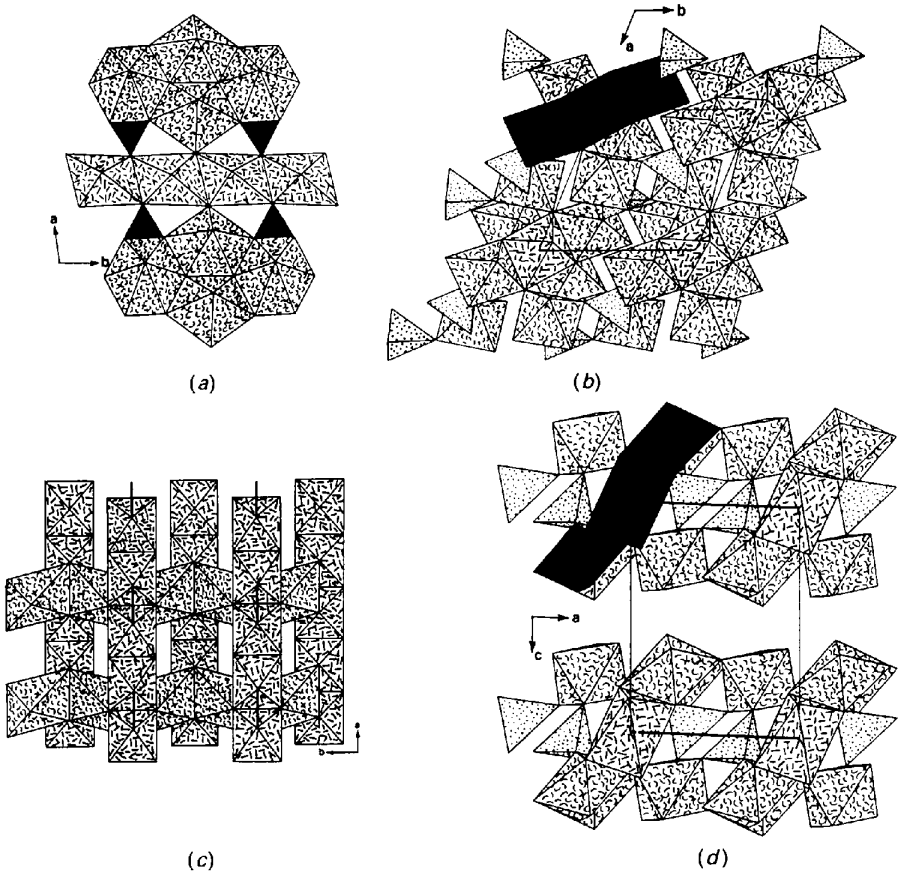

Fig. 10. Copper mineral structures with complex heteropolyhedral sheets: (*a*) roubaultite, in which chains of edge-sharing ($U\varphi_7$) and ($U\varphi_8$) pentagonal and hexagonal dipyramids cross-link through (CO_3) groups to edge-sharing [$Cu\varphi_4$] chains; the resulting sheet is parallel to (101), but is shown here projected onto (001); (*b*), (*c*) turquoise, with linear [$AlCuAl\varphi_{10}$] trimers (one trimer is shown in black) and [$Cu_2(PO_4)_2\varphi_8$] clusters corner sharing to form thick sheets parallel to (001); (*d*) likasite, a sheet of interlocking [$Cu\varphi_4$] chains cross-linked by (NO_3) groups seen edge-on in this view and denoted by thick lines.

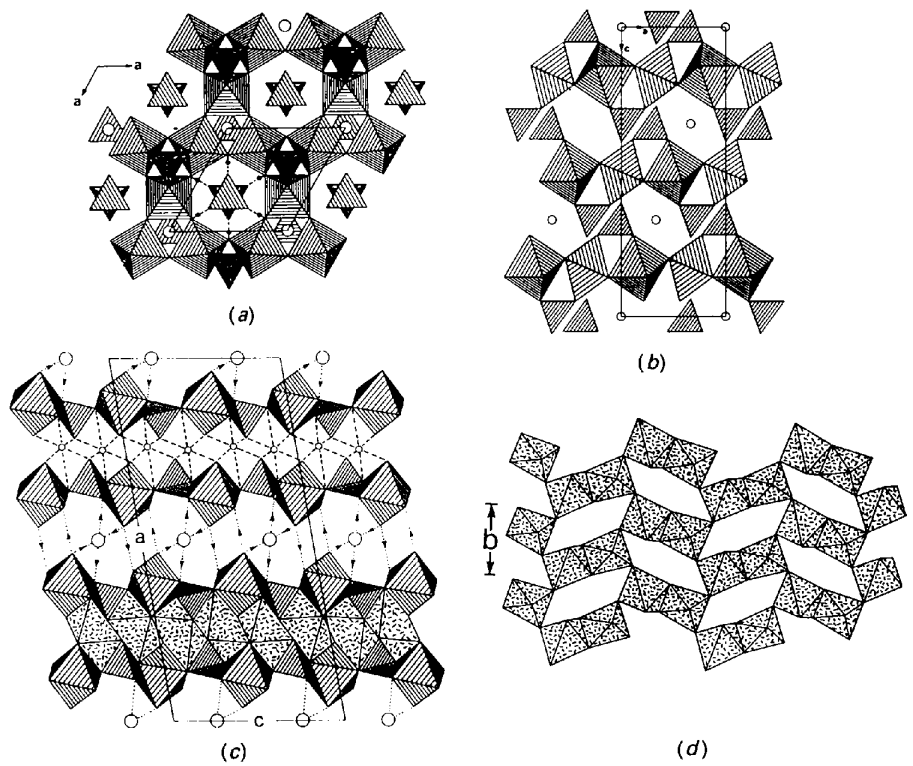

Fig. 11. Copper mineral structures with complex heteropolyhedral sheets: (*a*), (*b*) osarizawaite, a complex sheet of corner-sharing octahedra and tetrahedra; (*c*), (*d*) nissonite, a thick slab of three sheets, a central Cu sheet of dashed octahedra (*d*) sandwiched between two [$Mg(PO_4)\varphi_n$] sheets that are line-shaded; note that the ($Mg\varphi_6$) octahedra and (PO_4) tetrahedra share corners, (H_2O) groups are shown as large hollow circles.

disordered over the three available octahedral sites. If this is the case, it suggests at least limited solid solution between corkite [$PbAl_3(SO_4)_2(OH)_6$] and an ideal $PbCu_3(SO_4)_2(OH)_6$ end-member.

M=M=T sheet structures

In nissonite (Fig. 11*c*), a central sheet of ($Cu\varphi_6$) octahedra is sandwiched between two sheets of corner-sharing ($Mg\varphi_6$) octahedra and (PO_4) tetrahedra to form thick slabs parallel to (100). The central Cu sheet (Fig. 11*d*) has a pronounced commensurate modulation along [001] such that the sheet can link to the sandwiching heteropolyhedral sheets. Intercalated between these slabs are (H_2O) groups that provide linkage *via* a hydrogen-bonding network.

Infinite framework structures

This is by far the largest class of Cu^{2+} oxysalts, and is subdivided according to the principal polyhedral connectivities. The minerals and their crystallographic details are given in Table 4.

M=M framework structures

Atacamite, $CuCl(OH)_2$, consists of interpenetrating edge-sharing octahedral chains running parallel to [100] and [001] (Fig. 12*a*). Parise & Hyde (1986) also emphasize the similarities between atacamite and the octahedral part of the spinel structure. Paratacamite is another polymorph of this composition, and the structure is similar to that of atacamite, consisting of interpenetrating edge-sharing octahedral chains. The structure has hexagonal symmetry, and viewed down [001] (Fig. 12*b*) consists of edge-sharing sheets (of the dioctahedral mica type) that are offset such that a vacant site in one sheet matches up with the junction of three occupied octahedra in the adjacent sheet. The hexagonal symmetry exerts significant constraints on local relaxation. One Cu site has six symmetrically equivalent Cu—φ bonds, and another has a [2+4]-coordination (as compared to the usual [4+2]-coordination); this will be examined in more detail elsewhere.

Bellingerite consists of solitary ($Cu\varphi_6$) octahedra and [$Cu_2\varphi_{10}$] edge-sharing dimers, both of which link by edge sharing to ($I\varphi_5$), ($I\varphi_6$) and ($I\varphi_7$) polyhedra to form an edge-sharing framework. Salesite is somewhat similar. Distorted ($I\varphi_6$) octahedra share corners to form sheets with half of the possible cation sites occupied. These sheets are corner-linked to rutile-like edge-sharing chains of ($Cu\varphi_6$) octahedra to give a close-packed structure with the I sheets stacked along [100].

M—M=M T framework structures

Mammothite consists of euchroite-like chains of ($Cu\varphi_6$) octahedra, cross-linked into a framework by ($Al\varphi_6$) and ($Sb^{5+}\varphi_6$) octahedra (Fig. 13*a*). Within this framework are isolated (SO_4) tetrahedra (Fig. 13*b*), held in place by a network of hydrogen bonds; the framework is further strengthened by [9]-coordinate Pb^{2+}.

M—T framework structures

A prominent motif in the structure of bonattite is the simple *trans* vertex-sharing [$M(TO_4)\varphi_4$] chain in which octahedra and tetrahedra alternate along its length. In one view (Fig. 13*c*), these chains share vertices to form a sheet of six-membered rings of octahedra and tetrahedra. In another view (Fig. 13*d*), it can be seen that these chains are alternately skew to each other, and link by sharing corners to form a framework; if the chains were parallel, the same number of interchain linkages would only form sheets, such as the sheet module in newberyite [$Mg(PO_3OH)(H_2O)_3$] (Sutor, 1967; Hawthorne, 1990).

M—M—T framework structures

The structure of poitevinite has not been refined, but it is isostructural with kieserite (Hawthorne,

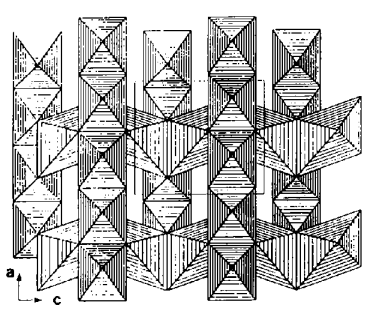

(*a*)

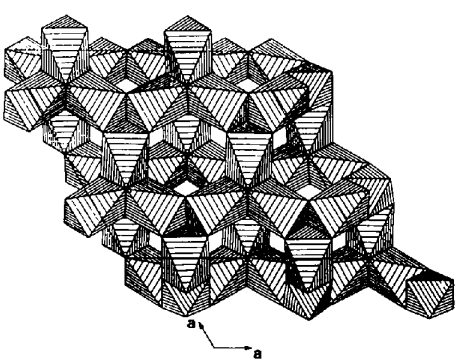

(*b*)

Fig. 12. Atacamite and paratacamite, octahedral framework structures: (*a*) viewed along [010], a framework of interpenetrating [$Cu\varphi_4$] chains; (*b*) viewed along [001], an offset series of edge-sharing octahedral sheets (*cf.* dioctahedral mica) stacked along [001].

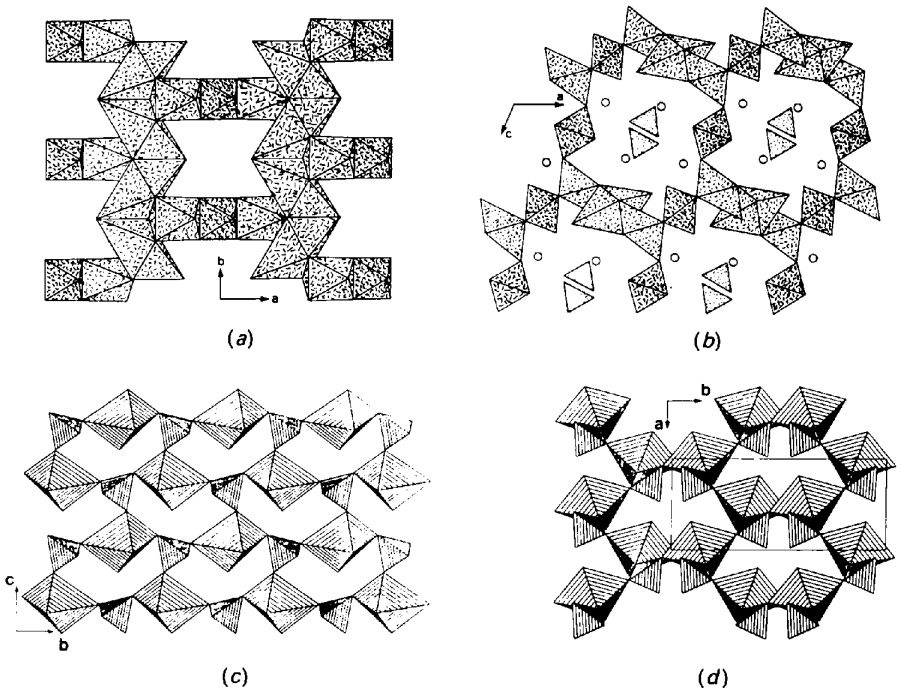

Fig. 13. Copper minerals with sparsely linked frameworks: (*a*), (*b*) mammothite, a framework of ($Cu\varphi_6$) octahedra (dashed), ($Al\varphi_6$) octahedra (curl shaded) and ($Sb^{5+}\varphi_6$) octahedra (dashed and dotted) with hydrogen-bonded interstitial (SO_4) groups (dotted); interstitial Pb atoms are shown by hollow circles; (*c*), (*d*) bonattite, a heteropolyhedral corner-sharing framework of ($Cu\varphi_6$) octahedra and (SO_4) tetrahedra.

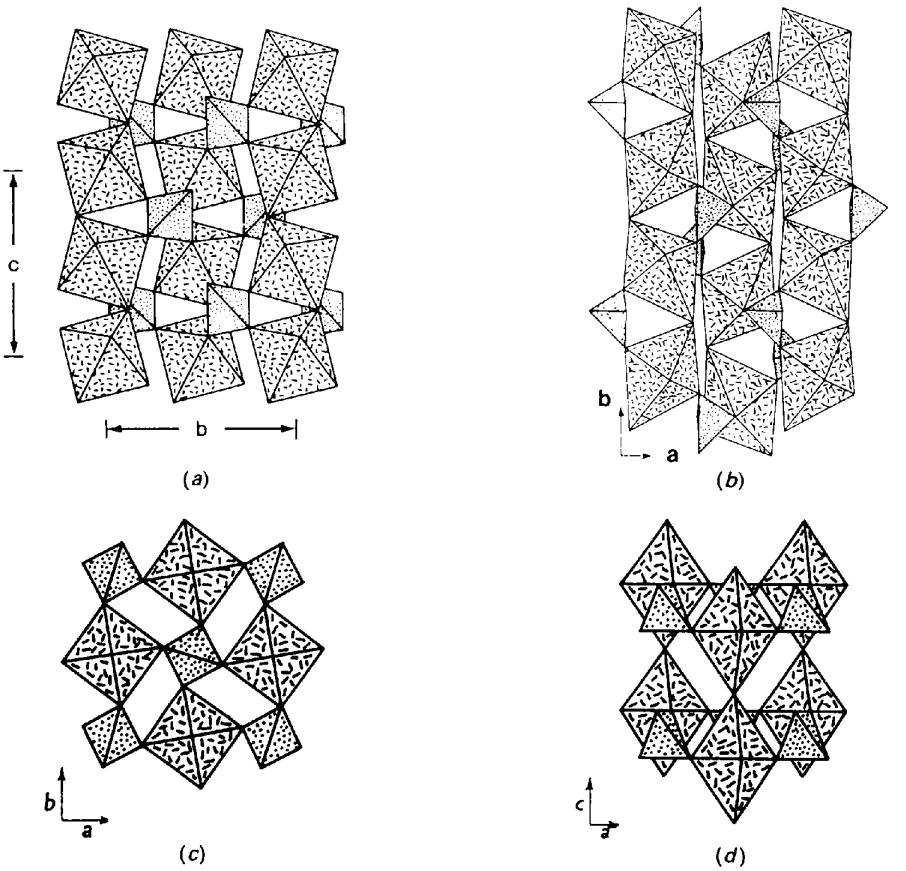

Fig. 14. Copper minerals with corner-linked frameworks: (*a*) poitevinite (actually the isostructural mineral kieserite), [$Cu\varphi_5$] chains (dashed) cross-linked by (SO_4) tetrahedra (dotted); (*b*) chalcomenite, drawn such as to show its similarities to the poitevinite structure; (*c*), (*d*) bandylite, [$Cu\varphi_5$] chains (dashed) cross-linked by ($B\varphi_4$) tetrahedra (dotted).

Groat, Raudsepp & Ercit, 1987). Corner-sharing $[M\varphi_5]$ octahedral chains run parallel to [001], and are cross-linked by tetrahedra to form a totally corner-linked framework; hydrogen bonding further strengthens the arrangement.

The structures of chalcomenite and teinite are similar to that of kieserite if we consider the Cu^{2+} as [6]-coordinate: a corner-sharing $[CuO_5]$ octahedral chain is flanked by (SeO_3) and (TeO_3) triangular pyramids, graphically very similar to the analogous unit in kieserite [except for the presence of triangular (SeO_3) pyramids instead of (SO_4) tetrahedra]. The principal difference is that (SeO_3) and (TeO_3) have one less vertex to share than (SO_4); the $(Cu\varphi_6)$ octahedra in the former structures have one unshared vertex [the source of the 'extra' (H_2O) group in chalcomenite and teinite relative to poitevinite].

Bandylite (Fig. 14*c*,*d*) consists of *trans* corner-sharing $[M\varphi_5]$ chains parallel to [001] and cross-linked by borate tetrahedra into a corner-linked framework. The tetrahedra link to four oxygens of the short meridional Cu—O bonds, and the long apical Cu—Cl bonds link along the octahedral chains.

M=M—T framework structures

A prominent motif in this group is the $[M\varphi_4]$ *trans* edge-sharing (rutile-like) octahedral chain that defines one direction with a repeat distance of $\sim 3n$ Å ($n = 1, 2...$). These chains are cross-linked by sharing edges and corners with octahedra from other chains, and also by sharing corners with tetrahedra or triangles (Fig. 15). Perpendicular to the length of the chain, these structures can be represented as a mapping of single triangles (corresponding to tetrahedra and/or triangles) and double triangles (corresponding to octahedra) on to the 3^6 net (Fig. 16); they are called wallpaper structures by Moore & Araki (1974). The Cu^{2+} oxysalt structures of this type are identified as such in Table 4.

The mixite-group minerals consist of single $[Cu\varphi_4]$ chains parallel to [001] (Fig. 15*a*), and cross-linked by arsenate or phosphate tetrahedra (Fig. 16*a*). The resulting arrangement has large channels containing disordered (H_2O) groups, and small channels containing the [9]-coordinate *A* cations.

Conichalcite also has single $[M\varphi_4]$ chains cross-linked by tetrahedra (Fig. 15*b*), but with a different arrangement to that in the mixite-group minerals. The channels apparent in Fig. 15(*b*) are occupied by [8]-coordinate Ca that provides additional linkage between the chains. Conichalcite is isostructural with several other non-Cu minerals (austinite, Ni-austinite, duftite). The structures of mottramite and calciovolborthite have not been refined, but they are isostructural with descloizite (Hawthorne & Faggiani, 1979). The type structure is similar to that of conichalcite (Fig. 15*b*), having single $[M\varphi_4]$ chains cross-linked by tetrahedra into a heteropolyhedral framework. The framework is graphically similar to that of conichalcite, differing only in the details of the interstitial cation coordination. Viewed perpendicular to the chain, we see that the flanking tetrahedra in descloizite and conichalcite (Fig. 15*b*) have a staggered configuration either side of the octahedral chain, in contrast to the arrangement in olivenite (Fig. 15*f*) in which the tetrahedra occur in a paired configuration.

The edge-sharing $[M\varphi_4]$ chain in euchroite is flanked by further octahedra in a staggered arrangement (Fig. 15*c*), and these chains cross-link by sharing corners with tetrahedra. In projection (Fig. 16*c*), these chains appear three octahedra wide and the tetrahedra and octahedra seem to be sharing edges, so it is important to examine both Figs. 15(*c*) and 16(*c*) to see the true linkage, clearly shown in Fig. 17(*a*).

In antlerite, $[M\varphi_4]$ chains share edges to form strips three octahedra wide, extending along [010] (Fig. 15*d*), and cross-linked by staggered sulfate tetrahedra (Fig. 16*d*). A view of the actual structure is shown in Fig. 17(*b*), where it can be seen that the octahedral strip flexes across its width, promoting axial extension of the central octahedra in line with the usual type of Jahn–Teller distortion.

Chalcocyanite and trippkeite both have rutile-like chains (Fig. 18), but the interchain linkage is not compatible with mapping onto a 3^6 net. In chalcocyanite, the chains have flanking tetrahedra linking both along and across the chains (Fig. 18*a*); the structure (Fig. 18*b*) appears as if it can be formed from ideal polyhedra, but can only link together if the polyhedra are extremely distorted. Trippkeite has triangular (AsO_3) pyramids, flanking the octahedral chain (Fig. 18*c*), and thus the amount of interchain linkage is less than in chalcocyanite. The resulting structure has channels (Fig. 18*d*) parallel to [001], into which the lone pairs of the As^{3+} project.

Lindgrenite (Figs. 18*e*, 18*f*) has strips of edge-sharing octahedra (Fig. 18*f*) parallel to [001], and cross-linked by (MoO_4) tetrahedra. Viewed down [001], the structure consists of close-packed heteropolyhedral layers that show a commensurate modulation along [010] (Fig. 18*e*) that allows the octahedra to assume a typical [4 + 2]-coordination while maintaining the connectivity of the close-packed arrangement.

The next series of structures have edge-sharing octahedral sheets linked by tetrahedra (Shoemaker & Kostiner, 1981). Cornubite consists of partly occupied octahedral sheets; each vacant octahedron is sandwiched between two opposing tetrahedra that

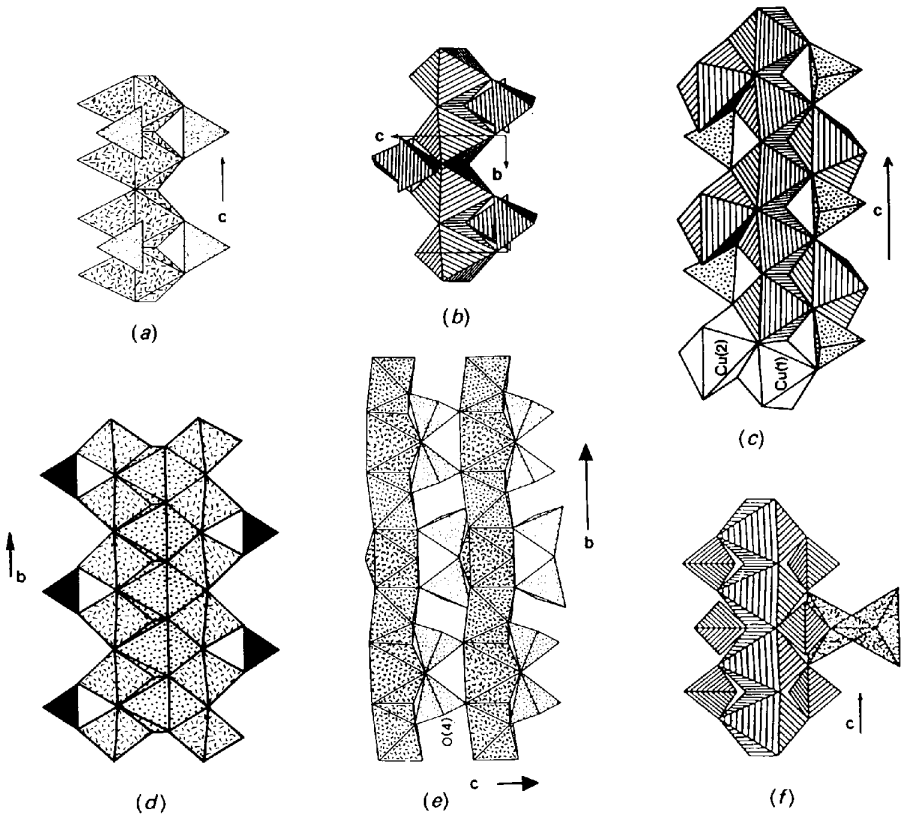

Fig. 15. Framework wallpaper structures showing the chain motif that is orthogonal to the 6^3 net; unless otherwise stated, tetrahedra are dot shaded, triangles are black and octahedra are dash or curl shaded: (*a*) mixite: (*b*) conichalcite, tetrahedra are line shaded; (*c*) euchroite; (*d*) antlerite, central ($Cu\varphi_6$) octahedra are dot shaded; (*e*) papagoite, curl shading denotes ($Ca\varphi_6$) octahedra; (*f*) olivenite, tetrahedra are line shaded, ($Cu\varphi_5$) polyhedra are dot shaded.

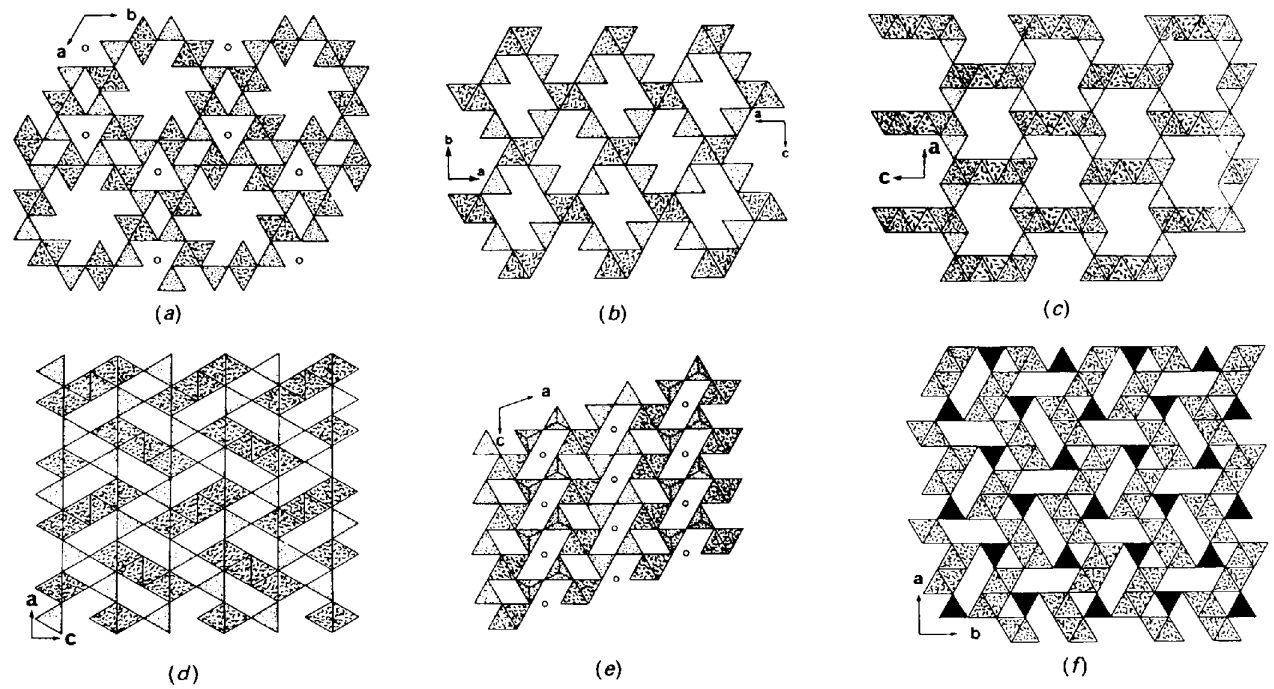

Fig. 16. Framework wallpaper structures (idealized) shown as monomeric and dimeric colourings of the 3^6 net; tetrahedra are dot shaded, triangles are black and octahedra are dash or curl shaded: (*a*) mixite; (*b*) conichalcite (left set of axes) and olivenite (right set of axes); (*c*) euchroite, note that octahedra and tetrahedra do not share edges (Fig. 17*a*); (*d*) antlerite; (*e*) papagoite; (*f*) malachite.

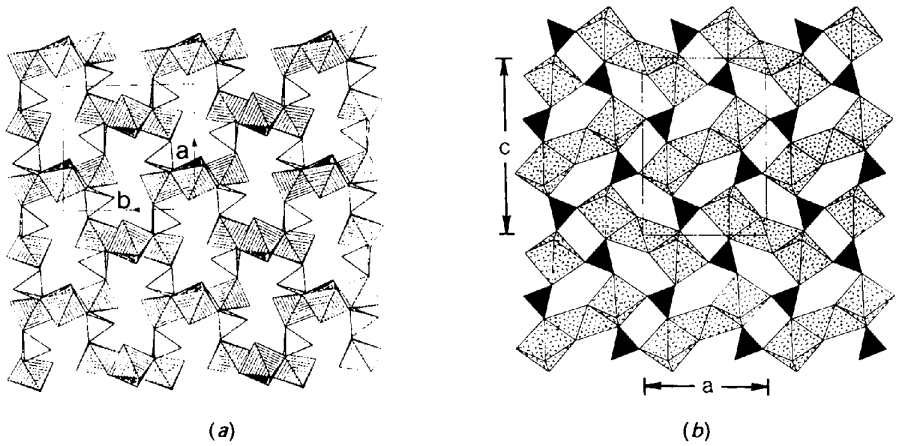

Fig. 17. The actual structural arrangements in (*a*) euchroite, octahedra are line shaded, tetrahedra are dot shaded; (*b*) antlerite, octahedra are dash and dot shaded, triangles are black; compare with Figs. 16(*c*) and 16(*d*) respectively.

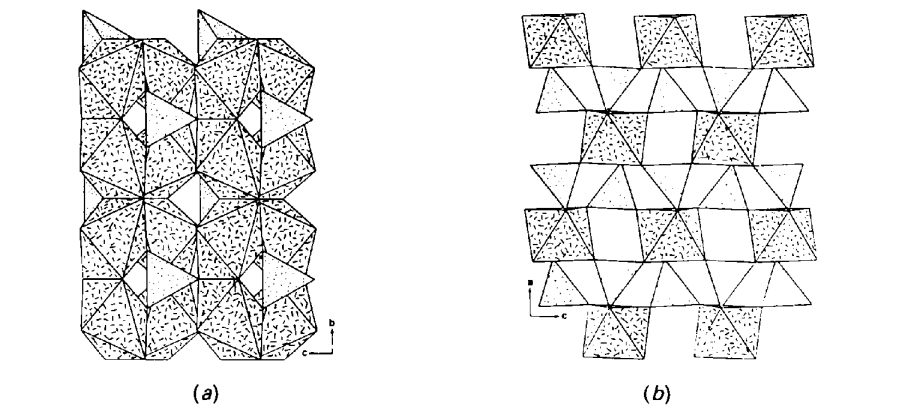

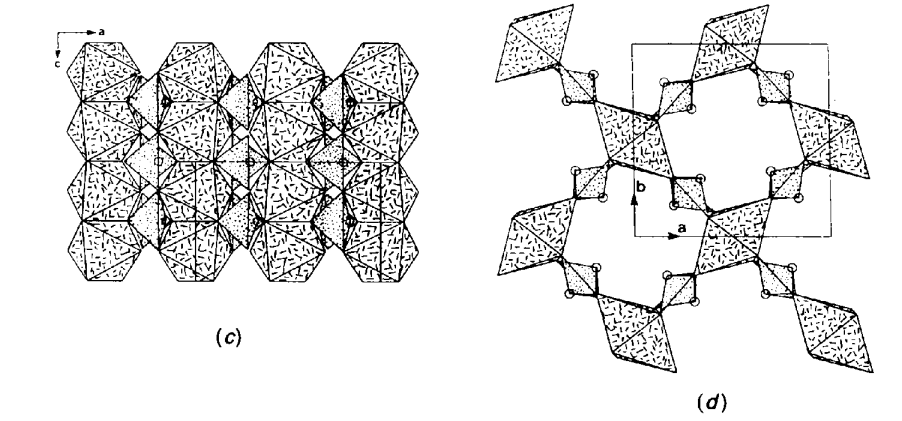

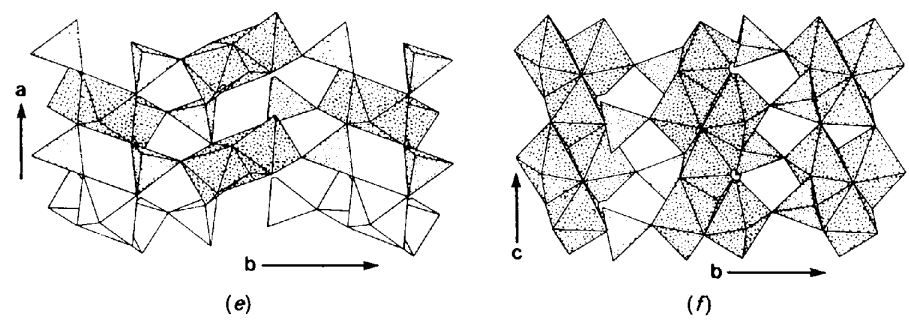

Fig. 18. Copper minerals with framework structures of edge-sharing octahedra and corner sharing between octahedra and tetrahedra: (*a*), (*b*) chalcocyanite, with $[Cu\varphi_4]$ chains cross-linked by (SO_4) tetrahedra; (*c*), (*d*) trippkeite, with $[Cu\varphi_4]$ chains cross-linked by (SeO_3) triangular pyramids, the arrangement producing large channels (*d*) into which the stereoactive lone pairs of the (SeO_3) groups protrude; (*e*), (*f*) lindgrenite, in which chains of edge-sharing $(Cu\varphi_6)$ octahedra are cross-linked by (MoO_4) tetrahedra. Octahedra are dash shaded, tetrahedra are dot shaded; in (*e*), one of the sheets in the close-packed arrangement is left unshaded to show the commensurate modulation of the structure along [010].

each share three vertices with the sheet. Adjacent sheets link through the fourth vertex of each tetrahedron. The stoichiometry $Cu_5(PO_4)_2(OH)_4.H_2O$ has three polymorphs: pseudomalachite, reichenbachite, and a synthetic (denoted QPM). All three structures have partly occupied octahedral sheets with different arrangements of vacancies; these vacancies always occur in edge-sharing pairs (Figs. 19*a*, 19*c*), and the different structures result from the different mappings of these dimers onto the octahedral sheet. The structures are rather unusual in that the linking tetrahedra share two vertices with each sheet (*e.g.* Fig. 20*a*) rather than the more usual three and/or one configuration (*e.g.* as in cornubite, Fig. 20*b*).

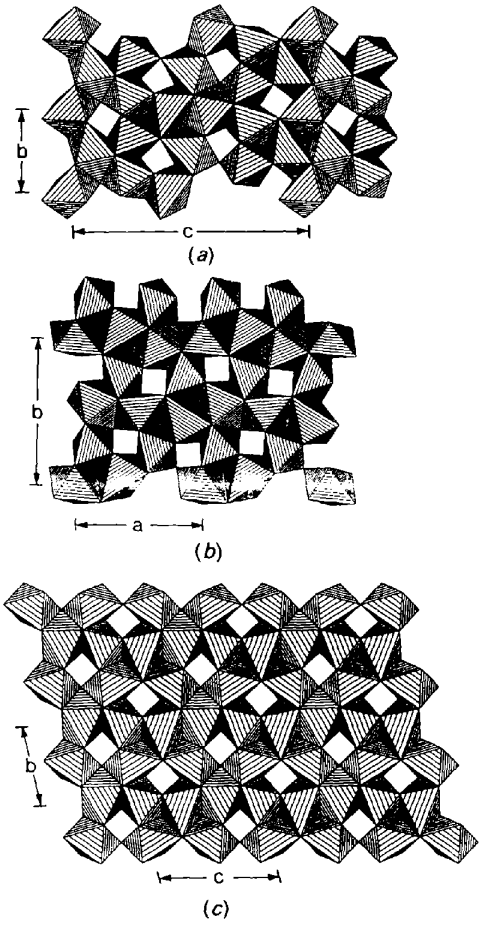

Fig. 19. Copper minerals with framework structures of edge-sharing octahedral sheets cross-linked by tetrahedra: (*a*) pseudomalachite; (*b*) reichenbachite; (*c*) the synthetic QPM; note that all the octahedral sheets are based on five-membered rings rather than the six-membered rings that are more usual in sheets of edge-sharing octahedra.

In mcbirneyite (Fig. 21*a*), partially occupied edge-sharing octahedral sheets parallel to (120) are cross-linked by corner sharing with tetrahedra and edge sharing with additional octahedra. A view of the structure down [120] (Fig. 21*b*) shows the sheet with the opposing pairs of tetrahedra on either side of each octahedral vacancy. Derriksite (Fig. 21*c*) also shows prominent edge-sharing octahedral sheets, alternating with chains of $(U\varphi_6)$ and (SeO_3) triangular pyramids; the octahedral sheets show a prominent modulation along [001] to encompass the typical Jahn–Teller distortion of the $(Cu\varphi_6)$ octahedra.

M—M=M—T framework structures

By and large, these structures are very similar to those of the previous group; linkages still tend to be dominated by the *M*=*M*—*T* motif, and the *M*—*M* linkage usually arises from a slightly different vacancy arrangement compared to *M*=*M*—*T* structures of similar type.

In malachite (Fig. 15*f*), $[M\varphi_4]$ chains share edges to form a strip two octahedra wide that extends along [001]. Each strip shares its apical vertices with the meridional vertices of adjacent strips, and further linkage is provided by (CO_3) triangles.

Arthurite (Fig. 22*a*) consists of complex heteropolyhedral sheets, cross-linked by isolated octahedra; it is isostructural with whitmoreite (Keller & Hess, 1978). The sheet is an octahedral edge-sharing $[M\varphi_3]$ sheet, but the distribution of vacancies (*i.e.* $[M_{1/2}\square_{1/2}\varphi_3]$) is such that some of the occupied octahedra share only corners. (AsO_4) tetrahedra link

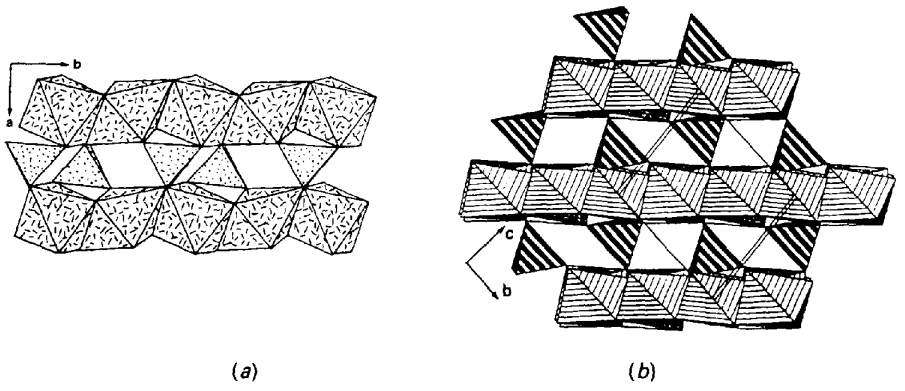

Fig. 20. Different types of cross-linkage of octahedral sheets by tetrahedra: (*a*) the synthetic QPM, with the tetrahedra (dot shaded) sharing two vertices with each sheet; (*b*) cornubite, in which the tetrahedra (striped) share three vertices with one sheet and one vertex with the other sheet.

outwards to isolated $[CuO_2(H_2O)_4]$ octahedra that provide linkage between the sheets, both directly and *via* hydrogen bonding.

Lammerite has edge-sharing chains of octahedra (α-PbO_2 type) extending along [100] and forming layers parallel to (001); within each layer, only alternate chains are occupied (Figs. 22*b*, 22*c*). These layers are cross-linked by arsenate tetrahedra and very distorted ($Cu\varphi_6$) octahedra. A commensurate modulation along [010] (Fig. 22*d*) allows the octa-

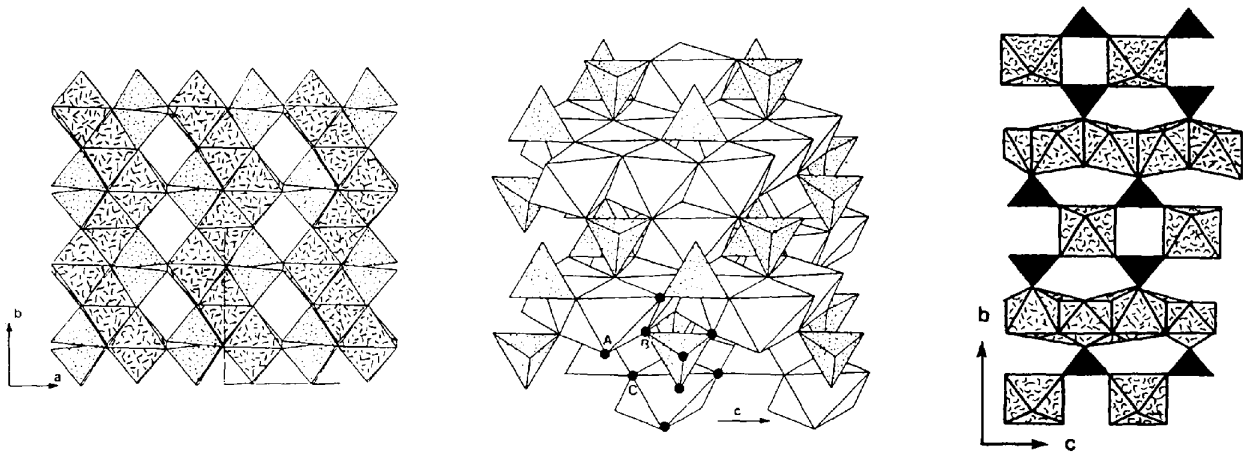

(*a*) (*b*) (*c*)

Fig. 21. Copper minerals with framework structures; (*a*), (*b*) mcbirneyite, a complex close-packed structure {(*b*) projected down [120]} of octahedra (dashed or blank) and tetrahedra (dotted); (*c*) derriksite, in which edge-sharing octahedral sheets (curl shaded)//(010) are interleaved with heteropolyhedral chains of ($U\varphi_6$) octahedra (dashed) and (SeO_3) triangular pyramids (black).

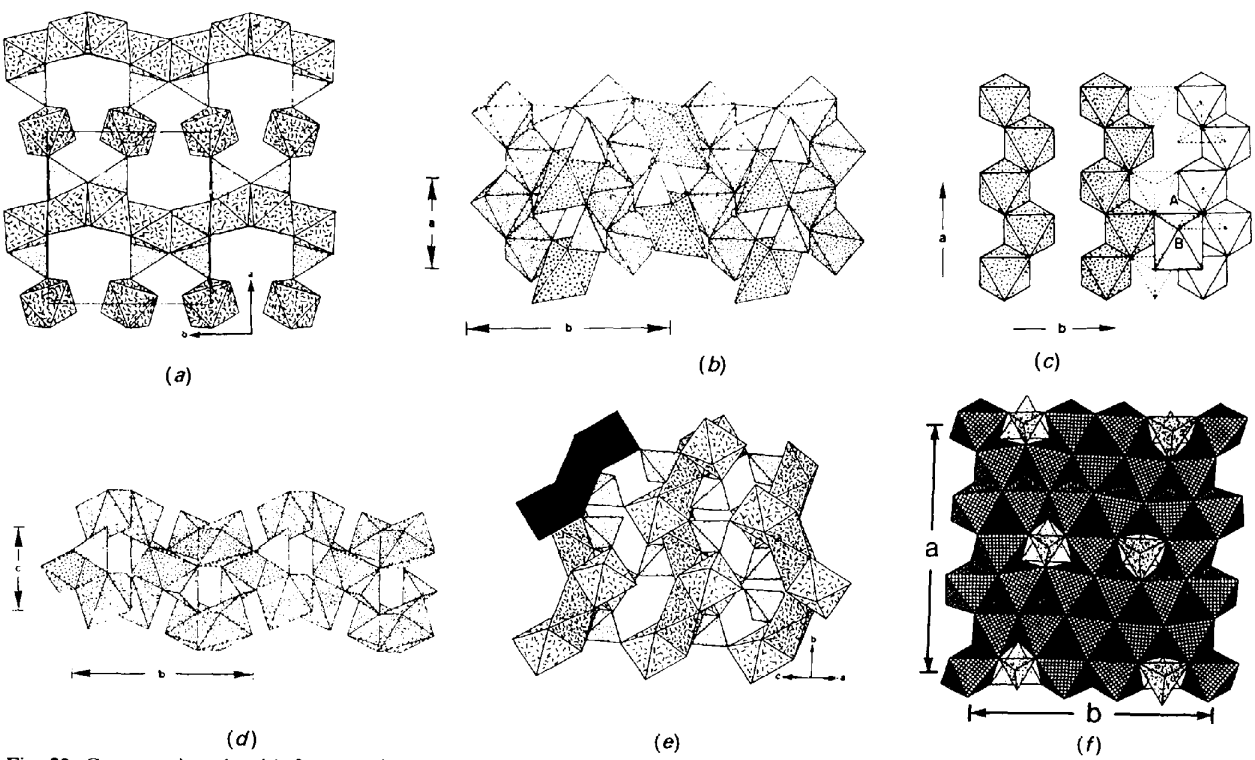

(*a*) (*b*) (*c*)

(*d*) (*e*) (*f*)

Fig. 22. Copper minerals with framework structures involving edge sharing between octahedra and corner sharing between octahedra and tetrahedra (dot shaded): (*a*) arthurite, with $[CuO_2(H_2O)_4]$ octahedra (curl shaded) cross-linking $[Fe^{3+}_2(AsO_4)_2(OH)_2]$ sheets; (*b*) the octahedral–tetrahedral layer in lammerite; ($Cu\varphi_6$) octahedra are dashed and large-dot shaded; (*c*) an idealized version of (*b*); (*d*) commensurate modulation of the close-packed sheets in lammerite; (*e*) hentschelite, with an [Al(dash)—Cu(curl)—Al(dash)] face-sharing octahedral trimer, one of which is shaded black; (*f*) the octahedral–tetrahedral sheet in ramsbeckite; small tetrahedra are (SO_4), large tetrahedra are (ZnO_4).

hedra to be distorted while maintaining their connectivity.

Hentschelite consists of Al—Cu—Al face-sharing octahedral trimers that are cross-linked into a framework by phosphate tetrahedra and by linking of adjacent trimers (Fig. 22*e*). Octahedral trimers adjacent along [101] are skew, and link in this direction by corner sharing between octahedra.

Ramsbeckite has an edge-sharing octahedral sheet with $\frac{2}{15}$ of the octahedral sites vacant (Fig. 22*f*), and decorated with (SO_4) and (ZnO_4) tetrahedra. One of the two sulfate tetrahedra shares vertices with the sheet and links across to a (ZnO_4) tetrahedron of the adjacent sheet. Further linkage is provided by intersheet hydrogen bonds.

In cornetite, ($Cu\varphi_6$) octahedra share edges to form staggered chains extending along [001] (Fig. 23*a*) that are linked into a complex sheet by edge sharing with [$Cu_2(PO_4)\varphi_6$] clusters along [010]. This sheet then links to the neighbouring sheet by sharing octahedron corners; in Fig. 23(*b*), alternate sheets are shaded and unshaded respectively, emphasizing the commensurate modulation of the sheet along [010].

M=M—T—T framework structures

Volborthite (Fig. 24*a*) has an edge-sharing octahedral sheet parallel to (001) with $\frac{3}{4}$ occupancy of the octahedral sites. Each octahedral vacancy is sandwiched between two (VO_4) tetrahedra that link through the fourth vertices of opposing tetrahedra in adjacent sheets.

In papagoite, the characteristic [$M\varphi_4$] chain consists of alternating ($Cu^{2+}\varphi_6$) and ($Al\varphi_6$) octahedra along [010] (Fig. 15*e*), cross-linked by corner sharing with four-membered corner-sharing silicate rings and edge-sharing ($Ca\varphi_6$) octahedra (Fig. 16*e*). In dioptase (Fig. 24*b*) six-membered corner-sharing tetrahedral rings linked by spiral chains of edge-sharing octahedra extend along [001].

Shattuckite (Fig. 25*a*) and plancheite (Figs. 25*b*, 25*c*) are chain silicates with strong affinities to the pyroxene and amphibole groups respectively (Evans & Mrose, 1977). Shattuckite has a corrugated sheet of edge-sharing octahedra (see edge-on in Fig. 25*a*) perpendicular to [010] and sandwiched between layers of pyroxene-like [SiO_3] vertex-sharing chains parallel to [001]. These thick layers are linked by very distorted ($Cu\varphi_6$) octahedra. The plancheite structure is very similar (Fig. 25*b*), except for the fact that the silicate chains are of the amphibole type (Fig. 25*c*), with an [Si_8O_{22}] stoichiometry.

Veszelyite has an edge-sharing octahedral sheet (Fig. 26*a*) in which the occupied octahedra form eight-membered rings around clusters of two vacancies. There is also a sheet of corner-sharing (ZnO_4) and (PO_4) tetrahedra linked such that the tetrahedral connectivity defines a 4.8^2 net; this tetrahedral pattern mimics exactly the pattern of occupied octahedra (Fig. 26*b*). Tetrahedra point in both direc-

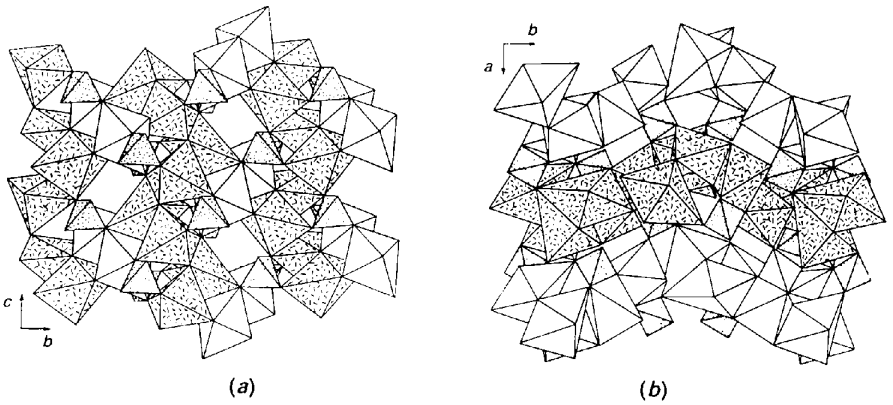

Fig. 23. The complex heteropolyhedral framework structure of cornetite: (*a*) projected down [010]; (*b*) projected down [001]; ($Cu\varphi_6$) octahedra are dash shaded, (PO_4) tetrahedra are dot shaded, and alternate layers are shaded and unshaded to show the commensurate modulation.

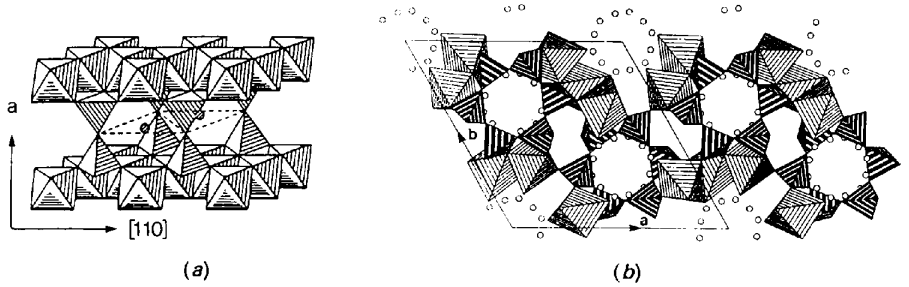

Fig. 24. Copper minerals with framework structures involving finite linkages between tetrahedra: (*a*) volborthite, with edge-sharing octahedral sheets cross-linked by [V_2O_7] pyro groups; (*b*) dioptase, with spiral chains of edge-sharing ($Cu\varphi_6$) octahedra (line shaded) cross-linked by [Si_6O_{18}] rings (stripes); interstitial (H_2O) groups are shown as circles.

tions perpendicular to the plane of the sheet, and link by sharing vertices with the sandwiching octahedral sheets (Fig. 26*c*). Kipushite also has a tetrahedral sheet in which (ZnO_4) and (PO_4) tetrahedra each occupy alternate vertices of a 4.8^2 net. The Cu cations occupy an edge-sharing octahedral sheet in which $\frac{1}{3}$ of the octahedra are empty. Two octahedral sheets are linked into a slab through one of the two distinct phosphate tetrahedra, together with hydrogen bonds from the hydroxyl anions coordinating the Cu^{2+} cations. The tetrahedral sheets are also linked in pairs to form a tetrahedral slab that links to the sandwiching octahedral slabs *via* corner sharing between both (ZnO_4) and (PO_4) tetrahedra and ($Cu\varphi_6$) octahedra.

Cu^{2+} in trigonal-prismatic coordination

Lyonsite (Table 5) has prominent face-sharing chains of ($Cu\varphi_6$) octahedra, all the vertices of which link to (VO_4) tetrahedra (Figs. 27*a*, 27*b*); the Cu sites are only half-occupied. The resultant columns extend along [001], and are linked together through chains of edge-sharing ($Fe\varphi_6$) octahedra and chains of edge-sharing ($Cu\varphi_6$) trigonal prisms (Fig. 27*b*). This coordination is extremely unusual for Cu^{2+}, consisting of four close oxygens ($\langle Cu—O\rangle = 1.97$ Å) in a square-planar arrangement, with two additional oxygens at 2.576 Å completing the trigonal prism (Hughes, Starkey, Malinconico & Malinconico, 1987).

[5]-coordinate Cu^{2+} structures

There are two types of coordination polyhedra with five vertices, the square pyramid and the triangular bipyramid. The former is the more common of the ($Cu^{2+}\varphi_5$) polyhedra, and it usually shares an edge with another square pyramid to form a [$Cu_2\varphi_8$] dimer. The structures in this group are listed in Table

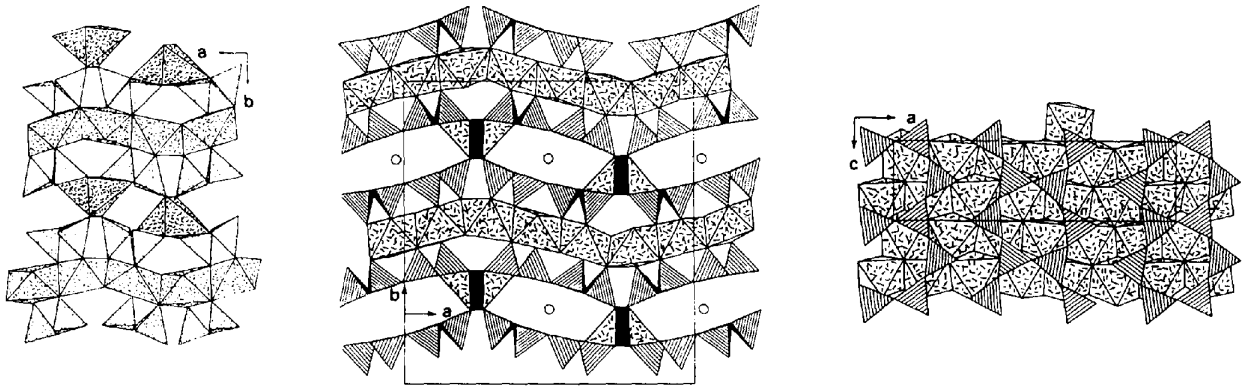

(*a*) (*b*) (*c*)

Fig. 25. Copper minerals with framework structures involving tetrahedral chains (dot or line shaded): (*a*) shattuckite, with modulated edge-sharing sheets of ($Cu\varphi_6$) octahedra (dash and curl shaded) linked by (pyroxene-like) corner-sharing [SiO_3] chains; (*b*), (*c*) plancheite, with similar modulated edge-sharing ($Cu\varphi_6$) sheets (dash shaded) linked by (amphibole-like) [Si_8O_{22}] chains. The black rectangles indicate the short meridional bonds of a very elongated ($Cu\varphi_6$) octahedron; possibly this Cu^{2+} cation is coordinated in a square-planar arrangement.

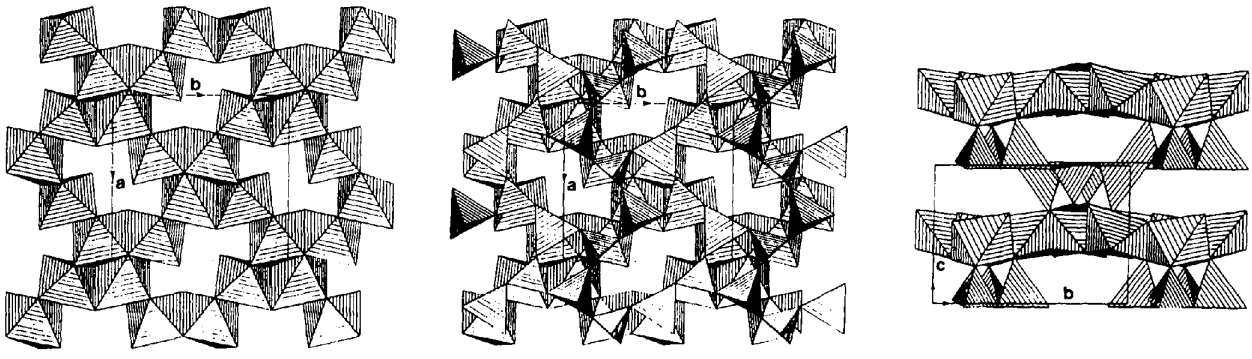

(*a*) (*b*) (*c*)

Fig. 26. The complex framework structure of veszelyite, involving tetrahedral sheets: (*a*) the edge-sharing sheet of octahedra with an unusual pattern of dimeric vacancies; (*b*) the matching of the octahedral sheet with a 4.8^2 net of corner-sharing (PO_4) and (ZnO_4) tetrahedra; (*c*) linkage of sheets along [001].

5. Unlike the structures with [6]-coordinate Cu^{2+}, these seem to be dominated by polymerized tetrahedral oxyanions.

Ziesite (β-$Cu_2V_2O_7$) (Fig. 28*a*) has edge-sharing [$Cu_2\varphi_8$] dimers sharing corners to form chains along [100] that are cross-linked by divanadate groups; it is isostructural with α-$Zn_2V_2O_7$ (Gopal & Calvo, 1972) and α-$Cu_2P_2O_7$ (Robertson & Calvo, 1968). At 985 K, ziesite transforms to blossite (α-$Cu_2V_2O_7$); there is a change in the coordination of the Cu cations, but the principal features of the structure remain the same.

Kinoite (Fig. 28*b*) is an elaborate structure. Chains of edge-sharing ($Cu\varphi_5$) square pyramids extend along [001], and chains adjacent in the [100] direction are linked by corner sharing with [Si_3O_{10}] trimers (Fig. 28*c*). This forms thick complex heteropolyhedral sheets parallel to (101) that are linked along [010] by [$Ca_2\varphi_{10}$] octahedral dimers to form a fairly open framework which is strengthened by additional hydrogen bonding.

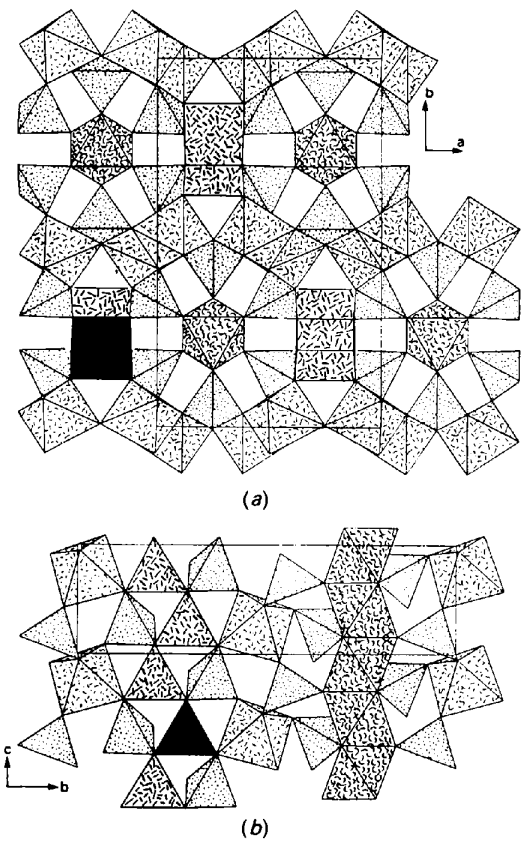

Fig. 27. The framework structure of lyonsite, with Cu^{2+} in both octahedral and trigonal prismatic coordination: (*a*) projected down [001], showing the 'pinwheels' of octahedra (curl shaded) and tetrahedra (dot shaded), cross-linked by Cu^{2+} in trigonal prismatic coordination (dash shaded); (*b*) projected down [100], showing the corner-linked chains of trigonal prisms extended along [001]; a single trigonal prism in each view is shaded black.

[4]-coordinate Cu structures

Cuprorivaite (Fig. 29*a*) consists of a puckered sheet of corner-linked (SiO_4) tetrahedra braced by ($Cu\varphi_4$) squares that share vertices with the tetrahedra such that the squares are parallel to sheets. The resultant sheets (or slabs) are linked by [8]-coordinate Ca (Fig. 29*b*).

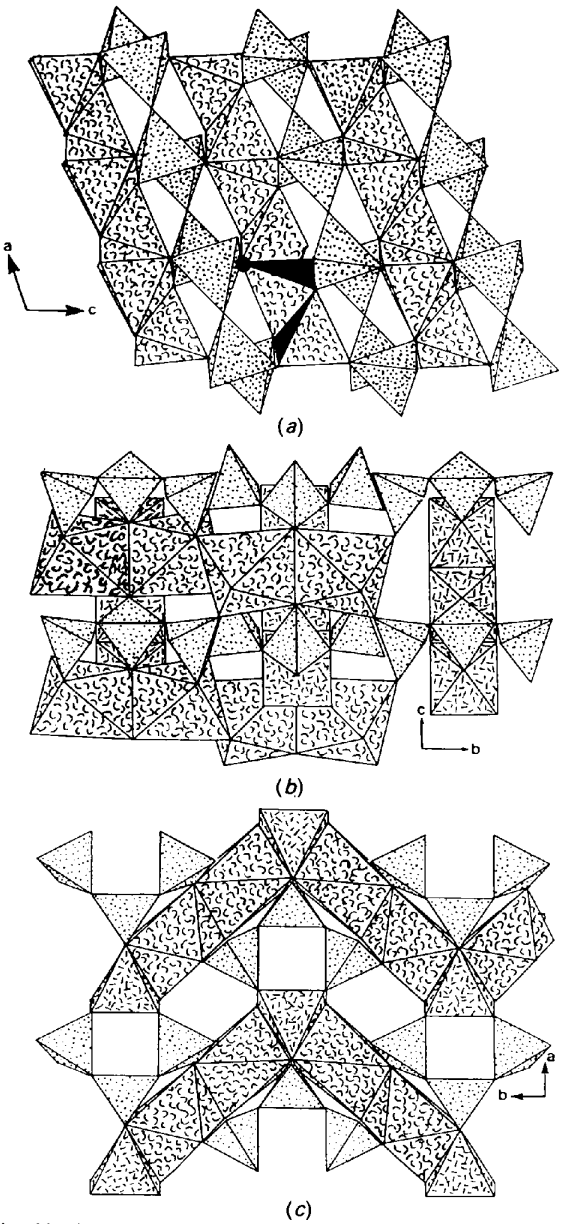

Fig. 28. Copper minerals with frameworks involving [5]-coordinate Cu^{2+}: (*a*) zeisite, with chains of corner-sharing [$Cu_2\varphi_8$] dimeric groups cross-linked by [V_2O_7] pyro groups (dot shaded; in the central chain, one dimer has two of its faces shaded black, and the corner-sharing vertex between two dimers is shown by a black circle); (*b*), (*c*) kinoite, with saw-chains of edge-sharing ($Cu\varphi_5$) square pyramids (dash shaded) cross-linked by [$Si_{13}O_{10}$] trimers (dot shaded) and edge-sharing ($Ca_2\varphi_{10}$) dimers (curl shaded).

[4]- and [6]-coordinate Cu structures

Azurite (Table 5) consists of edge-sharing chains of octahedra extending along [100] (Fig. 30*a*), cross-linked by (CO_3) and ($Cu\varphi_4$) groups to form a framework. This framework is stiffened by square-planar ($Cu\varphi_4$) groups (Fig. 30*b*) that cross-link four chains, and also share two corners with the (CO_3) groups.

Stringhamite (Table 5) has complex [$Cu(SO_4)$] sheets parallel to (010) and linked by interstitial Ca cations and (H_2O) groups (Fig. 30*c*). The sheets (Fig. 30*d*) consist of ($Cu\varphi_6$) octahedra that share edges and corners with (SO_4) tetrahedra to form chains parallel to [100]. These chains are then cross-linked along [001] by square-planar ($Cu\varphi_4$) groups which share corners with both tetrahedra and octahedra.

[5]- and [6]-coordinate Cu structures

Minerals in this particular group are listed in Table 5. All structures are of the type $M{=}M{-}T$, with edge sharing between Cu polyhedra, and corner sharing between Cu polyhedra and tetrahedra or triangles.

The structures of olivenite and libethenite are topologically the same, although libethenite is orthorhombic whereas olivenite is monoclinic. These are wallpaper structures with [$Cu\varphi_4$] chains of octahedra parallel to [001] (Fig. 15*f*), flanked by tetrahedra that cross-link adjacent chains. The resulting framework (Fig. 16*b*) is quite open, and the channels are filled with edge-sharing dimers of [5]-coordinate Cu^{2+}. This arrangement is fairly common, being found in such minerals as adamite, $Zn_2(AsO_4)(OH)$ (Hawthorne, 1976) and andalusite, $Al_2(SiO_4)O$ (Winter & Ghose, 1979).

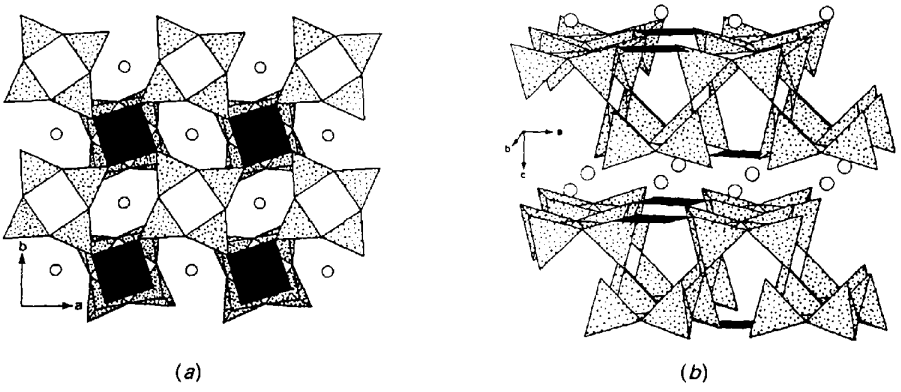

Fig. 29. Copper minerals with [4]-coordinate Cu^{2+}: (*a*), (*b*) the structure of cuprorivaite, a puckered sheet of (SiO_4) tetrahedra (dot shaded) reinforced by ($Cu\varphi_4$) squares (black).

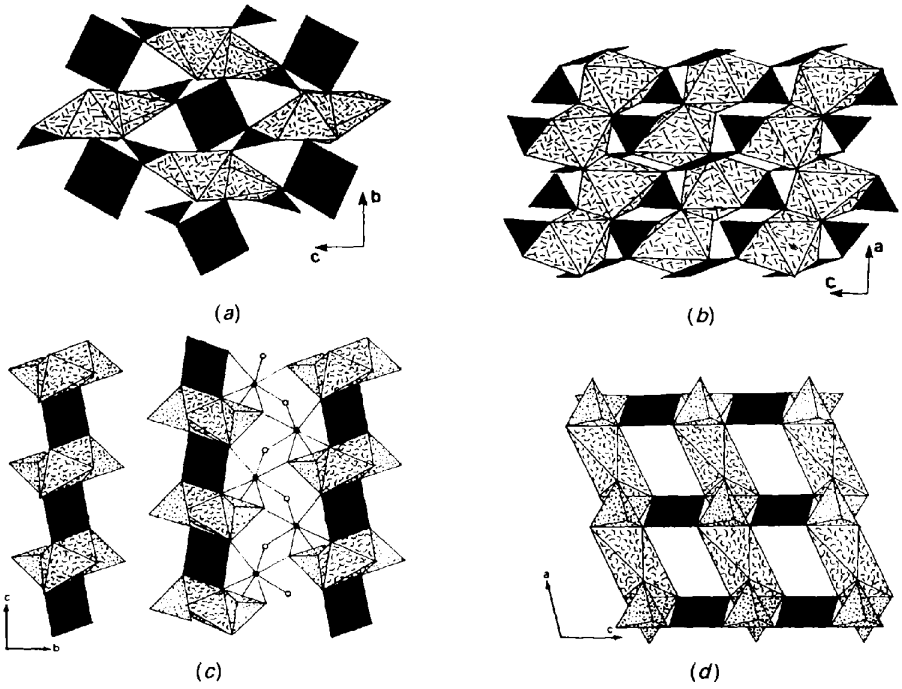

Fig. 30. Copper minerals with structures involving Cu^{2+} in both [4]- and [6]-coordination: (*a*), (*b*) azurite, with edge-sharing chains of ($Cu\varphi_6$) octahedra (dash shaded) cross-linked by ($Cu\varphi_4$) squares (black) and (CO_3) triangles (black); the extreme distortion makes the recognition of individual ($Cu\varphi_6$) octahedra difficult in (*a*); to help this, one octahedron in one of the chains (seen 'end-on' in this view) is not shaded; (*c*), (*d*) stringhamite, with sheets of ($Cu\varphi_6$) octahedra (curl shaded), ($Cu\varphi_4$) squares (black) and (SiO_4) tetrahedra (dot shaded), cross-linked by Ca (black circles) and (H_2O) groups (hollow circles).

Stranskiite has very distorted (CuO_6) octahedra that share edges with $[Zn_2\varphi_8]$ edge-sharing triangular-bipyramidal dimers to form staggered chains parallel to [010] (Fig. 31*a*), cross-linked by (AsO_4) tetrahedra. Alternatively, the structure can be described as a framework of six-membered ($Zn\varphi_5$)–(AsO_4) rings (Fig. 31*b*) with cross-linking ($Cu\varphi_6$) octahedra. Although the Cu is only octahedrally coordinated in stranskiite, this is not the case in a synthetic equivalent: $Cu_3(PO_4)_2$ is isostructural with stranskiite (Shoemaker, Anderson & Kostiner, 1977), and hence has Cu^{2+} in both [6]- and [5]-coordination.

Stoiberite (Birnie & Hughes, 1979) has edge-sharing double chains of ($Cu\varphi_6$) octahedra (Fig. 31*c*) extending along [010] and cross-linked by (VO_4) tetrahedra. Chains of edge-sharing octahedra and $[Cu_2\varphi_8]$ dimers of edge-sharing triangular bipyramids (Fig. 31*d*) extend along [001], interlacing with the orthogonal octahedral double chains. Further cross-linkage is provided by (VO_4) tetrahedra *via* corner sharing to form a fairly dense framework.

Fingerite (Figs. 32*a*, 32*b*) contains prominent $[M\varphi_2]$ sheets of edge-sharing octahedra; $\frac{5}{7}$ of the octahedra are occupied, with a resultant $[\square_2Cu_5O_{14}]$ stoichiometry. These sheets are cross-linked by ($Cu\varphi_5$) triangular bipyramids and (VO_4) tetrahedra.

Dolerophanite (Fig. 32*c*) is characterized by rutile-like $[M\varphi_4]$ chains of edge-sharing ($Cu\varphi_6$) octahedra extending along [010]; this chain is flanked by (SO_4) tetrahedra that link adjacent apical octahedral vertices in a staggered arrangement. This complex chain is graphically identical to the ($Cu\varphi_6$)–(AsO_4) chain in conichalcite (Fig. 15*b*). These chains link *via* corner sharing to form prominent heteropolyhedral walls parallel to (110). Sandwiched between the chains of each sheet are $[Cu_2\varphi_8]$ dimers that provide further linkage within each sheet, and provide the only cross-sheet linkage by sharing corners with (SO_4) tetrahedra (Fig. 32*d*) of the two adjacent sheets.

Cu^{2+} coordination in oxysalt minerals

Cu^{2+} shows a variety of coordinations in oxysalt minerals: (i) octahedral (distorted and apparently regular); (ii) square pyramidal; (iii) trigonal bipyramidal; (iv) square planar; (v) trigonal prismatic; (vi) [7]-coordinate.

There is an almost continuous range of coordination geometries from (i)–(iv), and consequently it is difficult to draw any obvious boundaries between the various coordinations. Indeed, it may be inappropriate to do so, as the presence or absence of a very weak interaction obviously has little energetic influence on a structure. However, the current re-

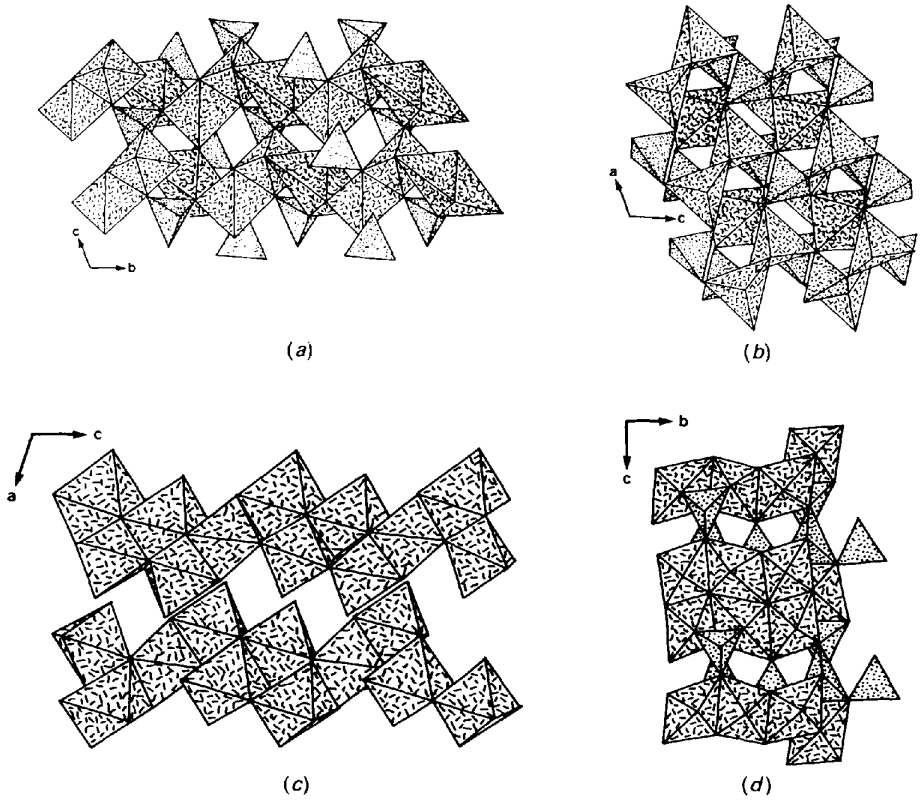

Fig. 31. Copper minerals with structures involving Cu^{2+} in both [5]- and [6]-coordination: (*a*), (*b*) stranskiite, a corner-sharing framework of $[Cu_2\varphi_8]$ edge-sharing dimers (dash shaded), ($Cu\varphi_6$) octahedra (curl shaded) and (AsO_4) tetrahedra (dot shaded); (*c*), (*d*) stoiberite (Shannon & Calvo, 1973), with corner-linkage between $[Cu\varphi_4]$ edge-sharing octahedral chains (dash shaded), $[Cu_2\varphi_8]$ dimers (curl shaded) and (VO_4) tetrahedra (dot shaded).

appraisal of most of the structural information does show that *intrinsic* octahedral coordination is dominant, and that many very distorted octahedral or [4]- or [5]-coordinations can be considered to be produced from a periodic structural distortion (*i.e.* an electron–phonon interaction) that effects a prototype structural arrangement involving regular octahedral coordination.

Octahedral coordination: orbital considerations

Jahn & Teller (1937) showed that any non-linear polyatomic molecule with an electronic orbital degeneracy is unstable. As a result, the molecule will spontaneously distort to split and/or lower the energy of one of the initially degenerate orbitals. The lower energy orbital will be occupied, the higher energy orbital will be unoccupied or partially occupied, and the amount of splitting of the initially degenerate orbitals is a measure of the stabilization energy of the system relative to that in the degenerate state. The specific details of this for Cu^{2+} (d^9 configuration) are easily sketched using ligand field theory. In a holosymmetric octahedral field, the d orbitals are split as shown in Fig. 33. The important point here is that the e_g orbitals are energetically degenerate, one being occupied by two (spin-paired) electrons and the other being occupied by a single electron. A net lowering of energy can be achieved by lifting the degeneracy of the e_g orbitals (Fig. 33). The lower-energy orbital is occupied by the spin-paired electrons, and the higher-energy orbital is occupied by the single electron, resulting in a new stabilization energy. As the symmetrical configuration has a higher energy than the unsymmetrical configuration, it is unstable with respect to the symmetry-lifting geometrical distortion that hence occurs spontaneously.

The Jahn–Teller theorem does not predict the geometrical nature of the distortion accompanying the lifting of the orbital degeneracy. However, simple shielding arguments (Burdett, 1982, 1986) show that a suitable distortion coordinate involves two *trans* bonds of the coordinating octahedron; these are designated as *axial* bonds. Shortening or lengthening of the axial bonds relative to the other four *equatorial* bonds lifts the orbital degeneracy of the holosymmetric coordination. These qualitative arguments do not indicate whether or not extention or contraction of the axial bonds is favoured. However, the refined crystal structures show extension of axial bonds (called a [4+2]-coordination) to be greatly preferred to the alternate [2+4]-coordination.

Octahedral coordination: observed stereochemistry

There is a very strong bimodal distribution of Cu—φ distances in the Cu^{2+} oxysalt minerals, with maxima at 1.97 and 2.44 Å and populations in the ratio 2:1 (Fig. 34). This supports the general idea of a [4+2]-distortion stabilizing octahedral coordination. Thus one can envisage an ideal distorted ($Cu^{2+}\varphi_6$) octahedron with an equatorial bond length of 1.97 Å and an axial bond length of 2.44 Å. Of course, local bond-valence requirements of specific bond topologies will perturb these values, and as expected, the dispersion of the axial bond lengths is much greater than that of the equatorial bond lengths (Dunitz &

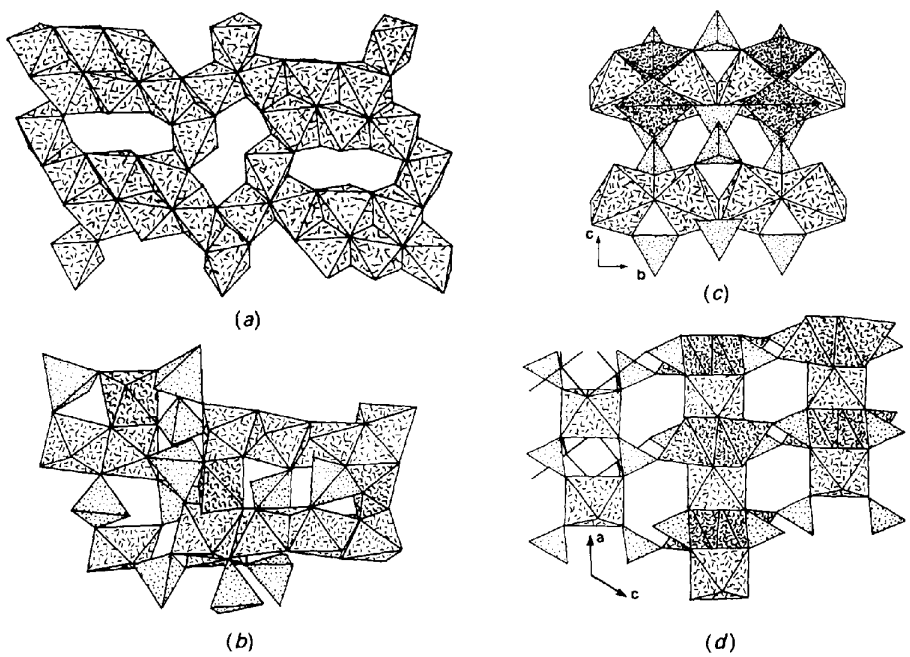

Fig. 32. Copper minerals with structures involving Cu^{2+} in both [5]- and [6]-coordination: (*a*), (*b*) fingerite, with edge-sharing sheets (*a*) of ($Cu\varphi_6$) octahedra (dash shaded) cross-linked (*b*) by ($Cu\varphi_5$) triangular bipyramids (curl shaded) and (VO_4) tetrahedra (dot shaded); (*c*), (*d*) dolerophanite, with edge-sharing [$Cu\varphi_4$] chains (dash shaded) flanked by (SO_4) tetrahedra (dot shaded) and cross-linking to [$Cu_2\varphi_8$] dimers (curl shaded).

Orgel, 1960), reflecting the 'softer' interaction at longer distances. Brown's (1981) bond-valence theorem indicates that such perturbations should be cooperative around each specific ion such that the sum of the incident bond valences is equal to the magnitude of the formal ion valence. This point is examined in Fig. 34. As the mean apical bond length increases, the mean equatorial bond length decreases in order to satisfy the local bond-valence requirements of the central Cu^{2+}. Brown & Shannon (1973) and Shannon & Calvo (1973) showed that the mean bond length of a specific cation–anion pair in a particular coordination can be affected by the degree of distortion from regularity of bond length. Accordingly, the Cu^{2+} oxysalt minerals (Fig. 35) show a linear relationship between bond-length distortion $\{\Delta = \Sigma[(l - l_0)/l]^2/6\}$ and mean bond length. The intercept value (for zero distortion) is 2.084 Å, indicating an ideal cation radius of 0.72 Å (for an average anion radius of 1.36 Å), close to the value of 0.73 Å assigned by Shannon (1976).

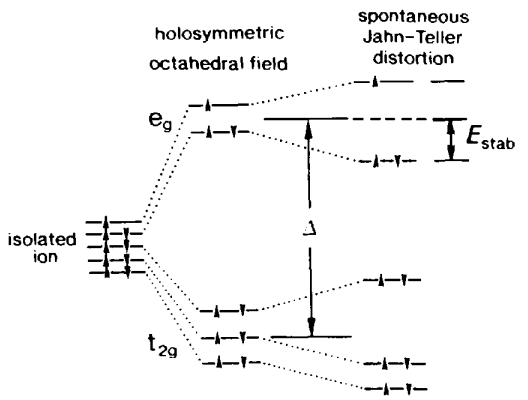

Fig. 33. *d*-orbital splittings in an octahedral and tetragonal ligand field; electron occupancies are for Cu^{2+} (d^9 configuration); note the splitting of the e_g levels induced by the tetragonal distortion, and the stabilization energy (E_{stab}) so produced.

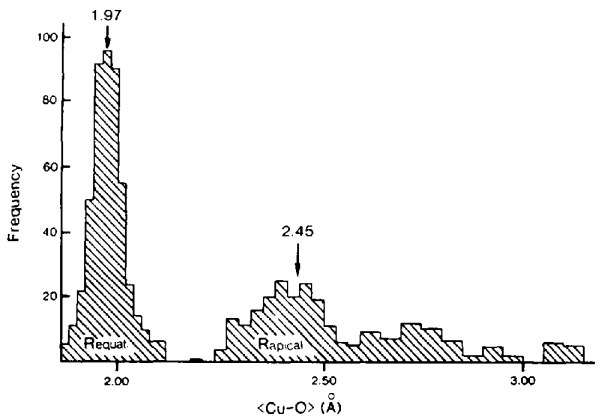

Fig. 34. Histogram of observed Cu—O distances in copper oxysalt minerals with octahedrally coordinated Cu^{2+}.

There are a few examples in which the $(Cu^{2+}\varphi_6)$ octahedron does not show the typical [4 + 2]-coordination. In paratacamite, Cu(1) lies on a sixfold axis and has six symmetrically equivalent bonds of 2.11 Å. In addition, Cu(2) has a [2 + 4]-coordination (*i.e.* an axially compressed octahedron). These two positions in the paratacamite structure are $\frac{1}{16}$ and $\frac{3}{16}$ of the total number of $(Cu\varphi_6)$ octahedra in the structure, and so are not quantitatively dominant; presumably the energetic advantage of this specific structural arrangement more than compensates for the energetic penalty of these unusual coordinations because of the small amount of Cu^{2+} ($\frac{1}{4}$) so affected.

Other examples of very regular octahedral coordination of Cu^{2+} are generally associated with partially occupied sites. In buttenbachite and connellite, the Cu(5) position lies on a sixfold axis; it is only half-occupied and the $\langle(Cu,\square)—\varphi\rangle$ distance is 2.25 Å. There are two possibilities here. The Cu may occupy a cavity too large for it, and its oribital degeneracy is relaxed (somewhat) by static or dynamic disorder about the central position. Alternatively the Cu(5) octahedron is smaller when occupied by the Cu and larger when unoccupied. If the latter is the case, then the energetic penalty of a regular Cu^{2+} coordination is offset by the fact that it only involves a small fraction of the Cu in the structure, and there is a compensating stabilization from the total structural arrangement. In lyonsite, there is partial occupancy of a site with quite regular (although not symmetrically constrained) octahedral coordination. Again there is the possibility of local relaxation around the occupied sites, and the lack of distortion only involves a small part of the structure, presumably offset by the gain in stabilization resulting from the complete structural arrangement.

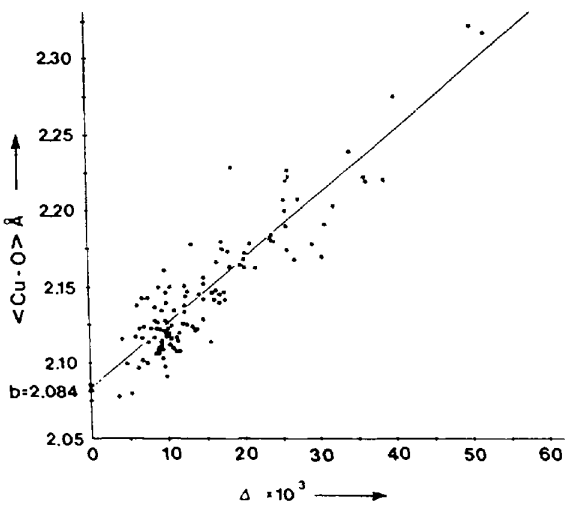

Fig. 35. Variation in $\langle^{[6]}Cu^{2+}—O\rangle$ as a function of bond-length distortion ($\Delta = \Sigma[(l - l_0)/l_0]^2/6$) in oxysalt minerals; the intercept of the regression line is 2.084 Å.

Thus to summarize, $^{[6]}Cu^{2+}$ usually shows [4+2]-coordination with ideal distances of 1.97 and 2.44 Å, respectively; the dispersion of the axial distances is usually greater than that of the equatorial distances. Regular octahedral coordination of Cu^{2+} is occasionally observed, but is usually associated with partially occupied sites (suggesting the possibility of local static or dynamic distortion). In addition, these cases invariably involve only small amounts of Cu^{2+} in the structure; presumably the local energetic destabilization is overcome by the total stabilization due to the overall structure.

Square-pyramidal and trigonal-bipyramidal coordinations

When Cu^{2+} is [5]-coordinate, there is no longer the question of orbital degeneracy. As [5]-coordination can be derived from octahedral coordination by removal of an axial ligand, there is no longer any orbital degeneracy. Consequently Cu^{2+} in [5]-coordination does not show the extreme bond-length distortions of Cu^{2+} in octahedral coordination.

There are two geometrically distinct [5]-coordinations in Cu^{2+}-oxysalt minerals: square pyramidal and trigonal bipyramidal. Eby & Hawthorne (1990) found that the two coordination geometries are reasonably distinct in minerals, although there seems to be no obvious reason for this; it may be due just to the small number of structures examined. Preliminary molecular orbital calculations for these geometries (Burns & Hawthorne, 1990) show no significant energy barrier between these two coordination geometries.

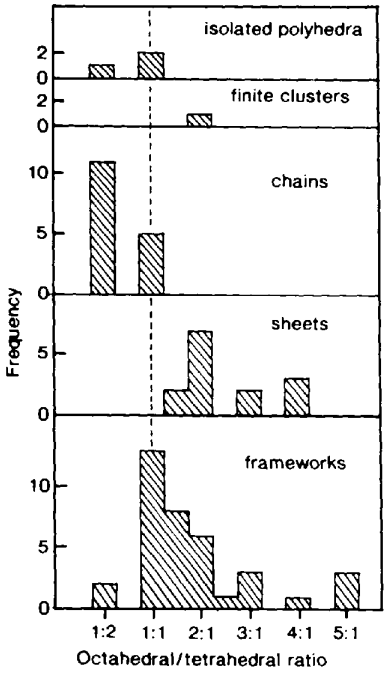

Fig. 36. Structure type as a function of the ratio of octahedra to tetrahedra in the Cu^{2+} oxysalt minerals.

Square-planar coordination

This is essentially the other end member of the [6]→[4+2]→[4] distortion series that lifts the orbital degeneracy of the regular ($Cu^{2+}\varphi_6$) group. In a transitional situation such as this, it is difficult to define where [4+2]-coordination becomes [4]-coordination. The minimum equatorial ⟨Cu—φ⟩ distances are 1.91 Å in cuprorivaite and 1.94 Å in several other structures. Possibly the former value is too short, although the bond-valence sums around Cu^{2+} in the other structures (azurite, stringhamite, paramelaconite, tenorite) are slightly low at ~1.91 v.u. However, taking 1.94 Å as the ideal (mean) value for square-planar Cu^{2+}, this suggests an axial bond 'cut-off' of ~3.1 Å for the boundary between [4+2]- and [4]-coordinations. There is very little dispersion in the individual $^{[4]}Cu—\varphi$ distances, as is usually the case for planar coordinations (Effenberger, 1985*a*).

Structural trends

Previous hierarchical schemes for specific classes of (mineral) structures have revealed systematic chemical trends as a function of structural connectivity. For the Cu^{2+}-oxysalt minerals, this point is examined in Fig. 36, which shows the various types of structures (frameworks, sheets, chains, *etc.*) as a function of octahedral:tetrahedral ratio. Several interesting features are evident in this figure. First, the distribution of compositions of the group as a whole seems to be centered about an octahedral: tetrahedral ratio of 1:1, a feature that is also true for all oxysalt structures. As yet, we see no persuasive reason for this, although it is obviously an important observation in terms of the general stability of inorganic structures.

For the isolated polyhedra and finite-cluster structures, there are too few examples to make any significant generalizations. However, this is not the case for the chain, sheet and framework structures. There is complete partitioning between the chain and the sheet structures, the former favouring tetrahedra and triangles, and the latter favouring octahedra. The framework structures show a greater range of composition, overlapping the ranges of both chain and sheet structures, but showing a greater concentration of structure types at the 1:1 and 2:1 compositions. These factors are currently under investigation as part of a general study of the relationships between heteropolyhedral connectivity and chemical composition in oxysalt structures.

This work was supported by the Natural Sciences and Engineering Research Council of Canada in the form of a Postgraduate Scholarship to RKE, and a University Research Fellowship, an Operating Grant and an Infrastructure Grant to FCH.

References

ALBRIGHT, T. A., BURDETT, J. K. & WHANGBO, M.-H. (1985). *Orbital Interactions in Chemistry*. New York: Wiley.

ANDERSON, J. B., SHOEMAKER, G. L., KOSTINER, E. & RUSZALA, F. A. (1977). *Am. Mineral.* **62**, 115–121.

ARUGA, A. & NAKAI, I. (1985). *Acta Cryst.* C**41**, 161–163.

ASAI, T. & KIRIYAMA, R. (1973). *Bull. Chem. Soc. Jpn*, **46**, 2395–2401.

BACON, D. E. & CURRY, N. A. (1962). *Proc. R. Soc. London*, **266**, 95–108.

BASSO, R., PALENZONA, A. & ZEFIRO, L. (1988). *Neues Jahrb. Mineral. Monatsh.* pp. 385–394.

BAUR, W. H. (1964). *Acta Cryst.* **17**, 1167–1174.

BAUR, W. H. & ROLIN, J. L. (1972). *Acta Cryst.* B**28**, 1448–1455.

BIRNIE, R. W. & HUGHES, J. M. (1979). *Am. Mineral.* **64**, 941–944.

BOVIO, B. & LOCCHI, S. (1982). *J. Crystallogr. Spectrosc. Res.* **12**, 507–517.

BROWN, G. M. & CHIDAMBARAM, R. (1969). *Acta Cryst.* B**25**, 676–687.

BROWN, I. D. (1981). *Structure and Bonding in Crystals*, Vol. 2, edited by M. O'KEEFFE & A. NAVROTSKY, pp. 1–30. New York: Academic Press.

BROWN, I. D. & SHANNON, R. D. (1973). *Acta Cryst.* B**29**, 566–585.

BRUNTON, G. (1973). *Am. Mineral.* **58**, 551.

BURDETT, J. K. (1982). *Adv. Chem. Phys.* **49**, 47–113.

BURDETT, J. K. (1986). *Mol. Struct. Energ.* **1**, 209–275.

BURNS, P. C. & HAWTHORNE, F. C. (1990). *Geol. Soc. Am. Annu. Meet. Abstr.* A259.

CALVO, C. & FAGGIANI, R. (1975). *Acta Cryst.* B**31**, 603–605.

CARAPEZZA, M. & RIVA DI SANSEVERINO, L. (1968). *Mineral. Petrogr. Acta*, **14**, 23–37.

CARAPEZZA, M. & RIVA DI SANSEVERINO, L. (1970). *Mineral. Petrogr. Acta*, **16**, 5–11.

CID-DRESNER, H. (1965). *Z. Kristallogr.* **121**, 87–113.

COCCO, G., FANFANI, L. & ZANAZZI, P. F. (1967). *Z. Kristallogr.* **124**, 385–397.

COLLINS, R. L. (1951). *Acta Cryst.* **4**, 204–209.

CORSDEN, A. (1978). *Can. Mineral.* **16**, 153–157.

DUNITZ, J. D. & ORGEL, L. E. (1960). *Adv. Inorg. Chem. Radiochem.* **2**, 1–60.

EBY, R. K. & HAWTHORNE, F. C. (1989*a*). *Acta Cryst.* C**45**, 1479–1482.

EBY, R. K. & HAWTHORNE, F. C. (1989*b*). *Mineral. Petrol.* **40**, 127–136.

EBY, R. K. & HAWTHORNE, F. C. (1990). *Acta Cryst.* C**46**, 2291–2294.

EFFENBERGER, H. (1977). *Tschermaks Mineral. Petrogr. Mitt.* **24**, 287–298.

EFFENBERGER, H. (1983). *Z. Kristallogr.* **165**, 127–135.

EFFENBERGER, H. (1985*a*). *Tschermaks Mineral. Petrogr. Mitt.* **34**, 279–288.

EFFENBERGER, H. (1985*b*). *Monatsh. Chem.* **116**, 927–931.

EFFENBERGER, H. (1986). *Neues Jahrb. Mineral. Monatsh.* pp. 101–110.

EFFENBERGER, H. (1987). *Mineral. Petrol.* **36**, 3–12.

EFFENBERGER, H. (1988). *Neues Jahrb. Mineral. Monatsh.* pp. 38–48.

EVANS, H. T. JR & MROSE, M. E. (1977). *Am. Mineral.* **62**, 491–502.

FANFANI, L., NUNZI, A., ZANAZZI, P. F. & ZANZARI, A. R. (1973). *Mineral. Mag.* **39**, 264–270.

FANFANI, L. & ZANAZZI, P. F. (1968). *Z. Kristallogr.* **126**, 433–443.

FINGER, L. W. (1985). *Am. Mineral.* **70**, 197–199.

FINNEY, J. J., GRAEBER, E. J., ROSENWEIG, A. & HAMILTON, R. D. (1977). *Mineral. Mag.* **41**, 357–361.

FLEET, M. E. (1975). *Acta Cryst.* B**31**, 183–187.

GENTSCH, M. & WEBER, K. (1984). *Acta Cryst.* C**40**, 1309–1311.

GHOSE, S., LEO, S. R. & WAN, C. (1974). *Am. Mineral.* **59**, 573–581.

GHOSE, S. & WAN, C. (1974). *Acta Cryst.* B**30**, 965–973.

GHOSE, S. & WAN, C. (1978). *Am. Mineral.* **63**, 172–179.

GHOSE, S. & WAN, C. (1979). *Acta Cryst.* B**35**, 819–823.

GIACOVAZZO, C., MENCHETTI, S. & SCORDARI, F. (1973). *Acta Cryst.* B**29**, 1986–1990.

GIACOVAZZO, C., SCANDALE, E. & SCORDARI, F. (1976). *Z. Kristallogr.* **144**, 226–237.

GINDEROW, D. & CESBRON, F. (1979). *Acta Cryst.* B**35**, 2499–2502.

GINDEROW, D. & CESBRON, F. (1985). *Acta Cryst.* C**41**, 654–657.

GIUSEPPETTI, G. & TADINI, C. (1980). *Neues Jahrb. Mineral. Monatsh.* **9**, 401–407.

GOPAL, R. & CALVO, C. (1972). *Can. J. Chem.* **51**, 1004–1009.

GROAT, L. A. & HAWTHORNE, F. C. (1987). *Tschermaks Mineral. Petrogr. Mitt.* **37**, 87–96.

GROAT, L. A. & HAWTHORNE, F. C. (1990). *Am. Mineral.* **75**, 1170–1175.

HARKER, D. (1936). *Z. Kristallogr.* **93**, 136–145.

HAWTHORNE, F. C. (1976). *Can. Mineral.* **14**, 143–148.

HAWTHORNE, F. C. (1979). *Can. Mineral.* **17**, 93–102.

HAWTHORNE, F. C. (1983). *Acta Cryst.* A**39**, 724–736.

HAWTHORNE, F. C. (1985*a*). *Am. Mineral.* **70**, 455–473.

HAWTHORNE, F. C. (1985*b*). *Can. Mineral.* **23**, 669–674.

HAWTHORNE, F. C. (1985*c*). *Mineral. Mag.* **49**, 85–91.

HAWTHORNE, F. C. (1985*d*). *Tschermaks Mineral. Petrogr. Mitt.* **34**, 15–24.

HAWTHORNE, F. C. (1986*a*). *Can. Mineral.* **24**, 625–642.

HAWTHORNE, F. C. (1986*b*). *Am. Mineral.* **71**, 206–209.

HAWTHORNE, F. C. (1990). *Z. Kristallogr.* **132**, 1–152

HAWTHORNE, F. C. & EBY, R. K. (1985). *Neues Jahrb. Mineral. Monatsh.* pp. 234–240.

HAWTHORNE, F. C. & FAGGIANI, R. (1979). *Acta Cryst.* B**35**, 717–720.

HAWTHORNE, F. C. & FERGUSON, R. B. (1975). *Acta Cryst.* B**31**, 1753–1755.

HAWTHORNE, F. C. & GROAT, L. A. (1985). *Am. Mineral.* **70**, 1050–1055.

HAWTHORNE, F. C., GROAT, L. A. & EBY, R. K. (1989). *Can. Mineral.* **27**, 205–209.

HAWTHORNE, F. C., GROAT, L. A., RAUDSEPP, M. & ERCIT, T. S. (1987). *Neues Jahrb. Mineral. Abh.* **157**, 121–132.

HAWTHORNE, F. C., KIMATA, M. & EBY, R. K. (1992). *Am. Mineral.* In the press.

HUGHES, J. M., STARKEY, S. J., MALINCONICO, M. L. & MALINCONICO, L. L. (1987). *Am. Mineral.* **72**, 1000–1005.

JAHN, H. A. & TELLER, E. (1937). *Proc. R. Soc. London Ser. A*, **161**, 220–236.

KELLER, P. & HESS, H. (1978). *Neues Jahrb. Mineral. Abh.* **133**, 291–302.

KELLER, P., HESS, H. & DUNN, P. J. (1979). *Tschermaks Mineral. Petrogr. Mitt.* **26**, 167–174.

LAUGHON, R. B. (1971). *Am. Mineral.* **56**, 193–200.

MELLINI, M. & MERLINO, S. (1978). *Z. Kristallogr.* **147**, 129–140.

MELLINI, M. & MERLINO, S. (1979). *Z. Kristallogr.* **149**, 249–257.

MERCURIO-LAVAUD, D. & FRIT, B. (1973). *C. R. Acad. Sci.* **277**, 1101–1104.

MEREITER, K. & PREISINGER, A. (1986). *Anz. Oesterr. Akad. Wiss. Math. Naturwiss. Kl.* **123**, 79–81.

MOORE, P. B. & ARAKI, T. (1974). *Am. Mineral.* **59**, 958–1004.

MOSSET, A., BONNET, J.-J. & GALY, J. (1978). *Z. Kristallogr.* **148**, 165–177.
NAKAI, I. (1986). *Am. Mineral.* **71**, 1236–1239.
NICHOLS, M. C. (1966). *Am. Mineral.* **51**, 267.
PABST, A. (1959). *Acta Cryst.* **12**, 733–739.
PARISE, J. B. & HYDE, B. G. (1986). *Acta Cryst.* C**42**, 1277–1280.
PERTLIK, F. (1975). *Tschermaks Mineral. Petrogr. Mitt.* **22**, 211–217.
PIRET, P., DECLERCQ, J.-P. & WAUTER-STOOP, D. (1980). *Bull. Minéral.* **103**, 176–178.
PIRET, P. & DELIENS, M. (1988). *Bull. Minéral.* **111**, 167–171.
PIRET, P., DELIENS, M. & PIRET-MEUNIER, J. (1985). *Can. Mineral.* **23**, 35–42.
QURASHI, M. M. & BARNES, W. H. (1963). *Can. Mineral.* **7**, 561–577.
RIBBE, P. H., GIBBS, G. V. & HAMIL, M. M. (1977). *Am. Mineral.* **62**, 807–811.
ROBERTSON, B. E. & CALVO, C. (1968). *Can. J. Chem.* **46**, 605–611.
ROSENZWEIG, A. & RYAN, R. R. (1975). *Am. Mineral.* **60**, 448–453.
ROSS, M., EVANS, H. T. JR & APPLEMAN, D. E. (1964). *Am. Mineral.* **49**, 1603–1621.
SABELLI, C. (1980). *Z. Kristallogr.* **151**, 129–140.
SABELLI, C. (1982). *Am. Mineral.* **67**, 388–393.
SABELLI, C. & ZANAZZI, P. F. (1968). *Acta Cryst.* B**24**, 1214–1221.
SABELLI, C. & ZANAZZI, P. F. (1972). *Acta Cryst.* B**28**, 1182–1189.
SHANNON, R. D. (1976). *Acta Cryst.* A**23**, 751–767.
SHANNON, R. D. & CALVO, C. (1972). *Can. J. Chem.* **50**, 3944–3949.
SHANNON, R. D. & CALVO, C. (1973). *Acta Cryst.* B**29**, 1338–1345.
SHOEMAKER, G. L., ANDERSON, J. B. & KOSTINER, E. (1977). *Am. Mineral.* **62**, 1042–1048.
SHOEMAKER, G. L., ANDERSON, J. B. & KOSTINER, E. (1981). *Am. Mineral.* **66**, 169–175.
SHOEMAKER, G. L. & KOSTINER, E. (1981). *Am. Mineral.* **66**, 176–181.
SIEBER, N. H., HOFMEISTER, W., TILLMANS, E. & ABRAHAM, K. (1984). *Fortschr. Mineral.* **62**, 231–233.
SÜSSE, P. (1972). *Z. Kristallogr.* **135**, 34–55.
SUTOR, D. J. (1967). *Acta Cryst.* **23**, 418–422.
TILLMANNS, E., HOFMEISTER, W. & PETITJEAN, K. (1985). *Bull. Geol. Soc. Finl.* **57**, 119–127.
TOMAN, K. (1977). *Acta Cryst.* B**33**, 2628–2631.
WILDNER, M. & GIESTER, G. (1988). *Mineral. Petrol.* **39**, 201–209.
WINTER, J. K. & GHOSE, S. (1979). *Am. Mineral.* **64**, 573–586.
ZAHROBSKY, R. F. & BAUR, W. H. (1968). *Acta Cryst.* B**24**, 508–513.
ZIGAN, F., JOSWIG, W. & SCHUSTER, H. D. (1977). *Z. Kristallogr.* **145**, 412–426.
ZIGAN, F. & SCHUSTER, H. D. (1972). *Z. Kristallogr.* **135**, 416–436.

Acta Cryst. (1993). B**49**, 56–62

Space-Group Determination of Human Tooth-Enamel Crystals

BY E. F. BRÈS*

Max-Planck-Institut für Metallforschung, Institut für Werkstoffwissenschaft, Seestrasse 92, *D* 7000 *Stuttgart* 1, *Germany*

D. CHERNS AND R. VINCENT

*H. H. Wills Physical Laboratory, University of Bristol, Bristol BS*8 1*TL, England*

AND J.-P. MORNIROLI

Laboratoire de Métallurgie Physique, Université de Lille 1, *Bâtiment C*6, 59 655 *Villeneuve d'Asc CEDEX, France*

(*Received* 9 *February* 1992; *accepted* 19 *June* 1992)

Abstract

In the present work, we have determined the space group of human tooth-enamel crystals using – for the first time for a biological crystal – convergent beam electron diffraction (CBED). The symmetries observed in the different patterns we have obtained lead us to the $P6_3/m$ hydroxyapatite space group. Disorder, most likely situated in the columns formed by the hydroxyl ions of the crystals, is suggested as a cause of weak intensity in the otherwise forbidden $000l$ (l odd) reflections and low visibility of first-order Laue zone (FOLZ) reflections in the CBED pattern from crystals oriented along the [0001] zone axis. A monoclinic phase was not observed.

Introduction

Human enamel is 96% by weight composed of an inorganic phase (Sicher, 1962), which consists of poorly crystalline carbonated hydroxyapatite crystals with an elongated prismatic shape (Voegel, 1978).

Hydroxyapatite (OHAP) is a mineral of chemical composition $Ca_4(1)Ca_6(2)(PO_4)_6(OH)_2$, whose Ca atoms occupy two series of nonequivalent sites; the

* On leave from INSERM U157, Faculté de Chirurgie Dentaire, Université Louis Pasteur, 1 place de l'Hôpital, 67000 Strasbourg, France.

0108-7681/93/010056-07$06.00